Monthly Notices of the ROYAL ASTRONOMICAL SOCIETY

MNRAS **494,** 3799–3827 (2020) doi:10.1093/mnras/staa764
Advance Access publication 2020 April 2

A Volume-limited Sample of Cataclysmic Variables from *Gaia* DR2: Space Density and Population Properties

A. F. Pala [1,2★] B. T. Gänsicke [2] E. Breedt [3] C. Knigge,[4] J. J. Hermes,[5] N. P. Gentile Fusillo,[1,2] M. A. Hollands,[2] T. Naylor [6] I. Pelisoli [7] M. R. Schreiber,[8] S. Toonen,[9] A. Aungwerojwit,[10] E. Cukanovaite,[2] E. Dennihy,[11,12] C. J. Manser,[2] M. L. Pretorius,[13,14] S. Scaringi [15] and O. Toloza[2]

[1] *European Southern Observatory, Karl Schwarzschild Straße 2, D-85748 Garching, Germany*
[2] *Department of Physics, University of Warwick, Coventry CV4 7AL, UK*
[3] *Institute of Astronomy, University of Cambridge, Cambridge CB3 0HA, UK*
[4] *School of Physics and Astronomy, University of Southampton, Southampton SO17 1BJ, UK*
[5] *Department of Astronomy, Boston University, 725 Commonwealth Avenue, Boston, MA 02215, USA*
[6] *School of Physics, University of Exeter, Stocker Road, Exeter EX4 4QL, UK*
[7] *Institut für Physik und Astronomie, Universitätsstandort Golm, Karl-Liebknecht-Straße 24/25, D-14476 Potsdam, Germany*
[8] *Instituto de Física y Astronomía, Millennium Nucleus for Planet Formation (NPF), Universidad de Valparaíso, 2360102 Valparaiso, Chile*
[9] *Institute for Gravitational Wave Astronomy, School of Physics and Astronomy, West Office 237, Birmingham B15 2TT, Edgbaston, UK*
[10] *Department of Physics, Faculty of Science, Naresuan University, Phitsanulok 65000, Thailand*
[11] *Department of Physics and Astronomy, University of North Carolina at Chapel Hill, Chapel Hill, NC 27599-3255, USA*
[12] *Southern Operations Center, Gemini Observatory, Casilla 603, La Serena, Chile*
[13] *Department of Astronomy, University of Cape Town, Private Bag X3, Rondebosch 7701, South Africa*
[14] *South African Astronomical Observatory, PO Box 9, Observatory 7935, Cape Town, South Africa*
[15] *Department of Physics and Astronomy, Texas Tech University, Lubbock, TX 79409-1051, USA*

Accepted 2020 March 17. Received 2020 March 17; in original form 2019 July 26

ABSTRACT

We present the first volume-limited sample of cataclysmic variables (CVs), selected using the accurate parallaxes provided by the second data release (DR2) of the European Space Agency *Gaia* space mission. The sample is composed of 42 CVs within 150 pc, including two new systems discovered using the *Gaia* data, and is (77 ± 10) per cent complete. We use this sample to study the intrinsic properties of the Galactic CV population. In particular, the CV space density we derive, $\rho = (4.8^{+0.6}_{-0.8}) \times 10^{-6}\,\mathrm{pc}^{-3}$, is lower than that predicted by most binary population synthesis studies. We also find a low fraction of period bounce CVs, seven per cent, and an average white dwarf mass of $\langle M_{\mathrm{WD}} \rangle = (0.83 \pm 0.17)\,\mathrm{M}_{\odot}$. Both findings confirm previous results, ruling out the presence of observational biases affecting these measurements, as has been suggested in the past. The observed fraction of period bounce CVs falls well below theoretical predictions, by at least a factor of five, and remains one of the open problems in the current understanding of CV evolution. Conversely, the average white dwarf mass supports the presence of additional mechanisms of angular momentum loss that have been accounted for in the latest evolutionary models. The fraction of magnetic CVs in the 150 pc sample is remarkably high at 36 per cent. This is in striking contrast with the absence of magnetic white dwarfs in the detached population of CV progenitors, and underlines that the evolution of magnetic systems has to be included in the next generation of population models.

Key words: stars: evolution – Hertzsprung–Russell and colour–magnitude diagrams – novae, cataclysmic variables – stars: statistics.

1 INTRODUCTION

Cataclysmic variables (CVs) are compact interacting binaries containing a white dwarf accreting from a Roche lobe filling donor star

★ E-mail: annafpala@gmail.com

(see Warner 1995 for a comprehensive review). In most systems, these companions are low-mass, late-type stars. If the white dwarf is not magnetized ($B \lesssim 1$ MG), the mass lost from the donor forms an accretion disc around the white dwarf. In the presence of stronger magnetic fields, the disc is either truncated at the magnetospheric radius of the white dwarf (1 MG $\lesssim B \lesssim 10$ MG) or is fully suppressed ($B \gtrsim 10$ MG). In these magnetic CVs, known as intermediate polars (IPs) and polars, respectively, the accretion flow follows the field lines and accretes on to the white dwarf at its magnetic poles.

The evolution of CVs is, as for all types of interacting binaries, dictated by orbital angular momentum losses (AMLs) and by the internal structure of the companion star (Paczynski & Sienkiewicz 1983; Rappaport, Verbunt & Joss 1983; Spruit & Ritter 1983; Knigge, Baraffe & Patterson 2011). In fact, the time-scale at which the secondary star loses mass is comparable to its thermal time-scale, resulting in a donor that is slightly out of thermal equilibrium and hotter and bloated compared to an isolated main-sequence star of the same mass. This deviation from thermal equilibrium is thought to be the cause of the major features observed in the CV orbital period distribution: the 'period gap' and the 'period minimum', as further detailed later.

As angular momentum is removed from the system, the orbital separation decreases and, consequently, CVs evolve from long to short orbital periods (Paczynski & Sienkiewicz 1983; Rappaport et al. 1983; Spruit & Ritter 1983). At long orbital periods ($P_{\rm orb} \gtrsim 3$ h), CV evolution is driven by magnetic wind braking (MB) and gravitational wave radiation (GWR). The ongoing mass transfer monotonously erodes the secondary star that, at $P_{\rm orb} \simeq 3$ h, becomes fully convective. In the standard framework of CV evolution, it is assumed that a reconfiguration of the magnetic fields on the donor results in a greatly reduced efficiency of MB from that point onwards, and the secondary star detaches from its Roche lobe. In the period range $2\,{\rm h} \lesssim P_{\rm orb} \lesssim 3$ h, the so-called period gap, the system evolves as a detached binary while still losing angular momentum through GWR. Observational support for the disrupted MB hypothesis is provided by the observed properties of the post-common-envelope binaries (PCEBs) in the period range $2\,{\rm h} \lesssim P_{\rm orb} \lesssim 3$ h (Schreiber et al. 2010; Zorotovic et al. 2016). At $P_{\rm orb} \simeq 2$ h, the orbital separation is such that the donor fills its Roche lobe again and the accretion process resumes.

Below the period gap, CVs keep evolving towards shorter orbital periods until they reach the period minimum, $P_{\rm orb} \simeq 80$ min. At this stage, the time-scale on which the secondary star loses mass becomes much shorter compared to its thermal time-scale. The donor is driven out of thermal equilibrium and stops shrinking in response to the mass-loss. Consequently, the system starts evolving back towards longer orbital periods, becoming a 'period bouncer'.

With MB being much more efficient than GWR in removing angular momentum from the system, CVs above the period gap are predicted to have mass accretion rate orders of magnitudes higher ($\dot{M} \sim 10^{-9} - 10^{-8}\,{\rm M}_{\odot}\,{\rm yr}^{-1}$; Spruit & Ritter 1983) than those of the CVs below the period gap ($\dot{M} \sim 5 \times 10^{-11}\,{\rm M}_{\odot}\,{\rm yr}^{-1}$; Patterson 1984). While this is roughly in agreement with the accretion rates estimated from observations (Townsley & Gänsicke 2009; Pala et al. 2017), the theoretical framework outlined above fails to reproduce a number of observational properties of the Galactic population of CVs: (i) the predicted fractions of CVs above and below the period gap ($\simeq$1 and $\simeq$99 per cent, respectively; de Kool 1992; Kolb 1993; Howell, Nelson & Rappaport 2001) are in clear disagreement with the observations (e.g. $\simeq$23 and $\simeq$77 per cent; Gänsicke et al. 2009; though the observed samples are typically magnitude limited, and hence biased towards more luminous CVs); (ii) period bouncers are expected to be the main component ($\simeq$40–70 per cent) of the present-day Galactic CV population, but only a small number of such systems have been identified (Patterson, Thorstensen & Kemp 2005; Littlefair et al. 2006; Unda-Sanzana et al. 2008; Patterson 2011; Kato et al. 2015, 2016; McAllister et al. 2017; Neustroev et al. 2017; Pala et al. 2018); and (iii) there are clues of the presence of additional AML mechanisms that are not accounted for by the standard model of CV evolution (Patterson 1998; Knigge et al. 2011; Schreiber, Zorotovic & Wijnen 2016; Pala et al. 2017; Zorotovic & Schreiber 2017; Belloni et al. 2018; Liu & Li 2019), although the physical origin of this enhanced AML is still unclear.

A key parameter that provides stringent constraints on the models of CV formation and evolution is their space density, ρ_0. Binary population synthesis studies carried out by de Kool (1992) and Politano (1996) suggested CV space densities of $\simeq 2 \times 10^{-5} - 2.0 \times 10^{-4}\,{\rm pc}^{-3}$. More recent works by Goliasch & Nelson (2015), which also accounts for the presence of CVs containing nuclear evolved donors, and by Belloni et al. (2018) provide an estimate of $\simeq (1.0 \pm 0.5) \times 10^{-5}$ and $\lesssim 2 \times 10^{-5}\,{\rm pc}^{-3}$, respectively, comparable to the earlier results.

These predicted values are systematically larger than those derived from observations. For example, Thomas & Beuermann (1998) used the *ROSAT* All-Sky Survey to infer $\rho_0 \simeq 6.1 \times 10^{-7}\,{\rm pc}^{-3}$ for polars. Later studies based on the *ROSAT* Bright Survey (RBS) and the *ROSAT* North Ecliptic Pole (NEP) suggested $\rho_0 = 4^{+6}_{-2} \times 10^{-6}\,{\rm pc}^{-3}$ (Pretorius, Knigge & Kolb 2007a; Pretorius & Knigge 2012). Most recently, Hernández Santisteban et al. (2018) estimated an upper limit on the space density of period bounce CVs from a search for eclipsing systems in Stripe 82 from the Sloan Digital Sky Survey (SDSS; York et al. 2000), finding $\rho_0 \lesssim 2 \times 10^{-5}\,{\rm pc}^{-3}$.

In the past, an accurate measurement of the CV space density has been challenged by the lack of accurate distances. In April 2018, the European Space Agency (ESA) *Gaia* space mission has delivered parallaxes for more than one billion stars in its second data release (DR2; Gaia Collaboration 2016, 2018), providing the first opportunity to construct a volume-limited sample of CVs and to derive their intrinsic properties. Schwope (2018) carried out the first application of the *Gaia* data in this context and, using the distances from *Gaia* for an X-ray selected sample of CVs from RBS, NEP, and *Swift*/BAT survey, derived the space densities of IPs, $\rho_0 < 1.3 \times 10^{-7}\,{\rm pc}^{-3}$, and non-magnetic CVs, $\rho_0 < 5.1 \times 10^{-6}\,{\rm pc}^{-3}$. These results are based on the assumptions that the X-ray selected sample is complete and representative of the intrinsic population. However, as discussed by Pretorius & Knigge (2012), it is possible that a large fraction of faint CVs may not have been detected in the RBS and NEP surveys, and that the space density derived from the corresponding X-ray selected CV sample could be easily underestimated by a factor of $\simeq$2.

Here, we present a study of the first volume-limited sample of CVs within 150 pc, selected by combining the *Gaia* DR2 parallaxes and the available information from a large number of spectroscopic and photometric surveys.

The sample contains a total of 42 objects and provides the first direct insight into the intrinsic properties of the Galactic population of CVs.

2 SAMPLE SELECTION

The *Gaia* space mission provides the first opportunity to construct a volume-limited sample of CVs that allows us to infer the intrinsic properties of the Galactic CV population.

The first step towards this goal is the choice of an optimal volume, which is sufficiently large to be representative of the entire CV population and robust against small number statistics, and not subject to distance (magnitude)-related observational biases.

The volume enclosed within 150 pc represents a good compromise between the two requirements: assuming the typical space density derived from binary population synthesis studies, $\lesssim 2 \times 10^{-5}$ pc^{-3} (Belloni et al. 2018), it is expected to contain $\simeq$140 CVs, and at $d = 150$ pc even the systems with the lowest accretion rates[1] should be bright enough to have accurate astrometric solutions (typical uncertainties on the parallaxes are $\simeq$0.2 mas for $G \lesssim 19$ mag; see fig. 7 in Gaia Collaboration 2018). Restricting $d \leq 150$ pc also reduces the uncertainties in the derived space densities related to the unknown age and scale height of the CV population (see Section 3).

The next step is to compile a list of all CVs and CV candidates that could plausibly be within $d \leq 150$ pc. CVs are mainly discovered thanks to their outbursting properties. In fact, CV accretion discs undergo thermal instabilities called dwarf nova outbursts (Osaki 1974; Meyer & Meyer-Hofmeister 1984; Hameury et al. 1998), during which CV systems brighten up to 2–9 mag and these outbursts can last for days up to weeks (Maza & Gonzalez 1983; Warner 1995). Many surveys search the sky nightly for transient events, such as the Catalina Real-time Transient Survey (CRTS; Drake et al. 2009), the All-Sky Automated Survey and the All-Sky Automated Survey for Supernovae (ASAS and ASAS-SN; Pojmanski 1997; Shappee et al. 2014; Kochanek et al. 2017), the Mobile Astronomical System of TElescope Robots (MASTER; Lipunov et al. 2010), the Palomar Transient Factory (PTF; Law et al. 2009) and the Intermediate PTF (Kulkarni 2013), the Asteroid Terrestrial-impact Last Alert System (ATLAS; Tonry et al. 2018), the Zwicky Transient Facility (ZTF, Graham et al. 2019), and the *Gaia* Photometric Science Alerts (Hodgkin et al. 2013), which have been very successful in the identification of thousands of CVs in outbursts (e.g. Breedt et al. 2014).

Alternatively, CVs can be identified thanks to their blue colours (see e.g. Gänsicke 2005) and their X-ray emission (the latter favouring magnetic systems since the X-ray emission arises mainly from small, hot region near the magnetic poles of polars and IPs). Finally, CVs are one of the by-products of SDSS, with over 300 new CVs discovered in the last decade via the detection of strong emission disc lines in their spectra (Szkody et al. 2002, 2003, 2004, 2005, 2006, 2007, 2009, 2011). While the spectroscopic method is less affected by selection biases, it is the most expensive in terms of telescope time.

New systems are continuously discovered and an up-to-date catalogue of these discoveries is missing. We therefore searched the catalogues of the aforementioned transient surveys and the International Variable Star Index [VSX, Watson, Henden & Price 2006, compiled by the American Association of Variable Star Observers (AAVSO)] to collect all information regarding newly identified CVs and CV candidates. Combining these findings with the Ritter and Kolb catalogue (Ritter & Kolb 2003), a collection of the observational properties of all CVs with an orbital period determination (1429 systems), we built a list of $\simeq$8000 systems.

We cross-matched this list with the *Gaia* DR2 catalogue. In order to take into account proper motions and the low precision ($\simeq$10 arcsec) of the coordinates reported in some of the catalogues, we first performed a cross-match with a 30 arcsec search radius, resulting in $\simeq$364 000 objects. Using the *Gaia* proper motions and radial velocities (whenever available), we calculated the corresponding coordinates at epoch 2000. We then performed a second cross-match between our list of CVs and this catalogue, selecting the closest source within 10 arcsec radius, which resulted in $\simeq$6400 objects. Since our focus is on the properties of the 150 pc CV sample, we applied a cut in parallax:

$$\varpi + 3\sigma_{\varpi} \geq 6.66 \text{ mas}. \quad (1)$$

This selection returned 166 systems that, within their parallax uncertainties, are located within 150 pc (Fig. 1).

More than half of these 166 systems have been identified as CV candidates in transient surveys because they have shown one or more brightenings that resembled a dwarf nova outburst, but have no photometric or spectroscopic follow-up confirming their CV nature. Therefore, for each system, we inspected the literature, the CRTS, AAVSO, and ASAS-SN light-curve archives for their outburst history, and SDSS for serendipitous spectroscopy. In this way, we identified 28 objects that are mistakenly classified as CVs or CV candidates in the literature (Table D1), many of them single low-mass stars that show flaring phenomena that can be mistaken for dwarf nova outbursts. More details are provided in Appendices A, B, and C.

Finally, we searched for *Gaia* sources in the white dwarf locus of the Hertzsprung–Russell diagram (defined by the colour cuts from Hollands et al. 2018; see their equations 2–4) that showed large anomalous uncertainties in their G magnitudes, weighted over the number of observations in the given band. Such large values can be interpreted as intrinsic stellar variability arising from e.g. pulsations, debris transits, magnetism, or ongoing accretion (Hermes et al., in preparation). Among the different candidates, two systems stood out because of their large intrinsic variability and for being overluminous to the canonical white dwarf cooling tracks. Spectroscopic follow-up later confirmed these as new CVs located within 150 pc: *Gaia* J051903.99+630340.4 and *Gaia* J154008.28−392917.6 (Fig. 2 and Appendix D, which we named with the identifier *Gaia* JHHMMSS.SS±DDMMSS.S, defined with respect to their coordinates at equinox 2000 and epoch 2000, as computed using the *Gaia* ICRS coordinates and proper motions).

2.1 Astrometric accuracy

Along with positions, magnitudes, and proper motions, i.e. the kinematic parameters used to obtain the astrometric solution for each source, *Gaia* DR2 provides a series of additional parameters that allow to evaluate the accuracy of this solution. In particular, the `astrometric_excess_noise` (AEN) represents the errors introduced in the astrometric modelling (see Lindegren et al. 2012) and, ideally, should be zero. A possible selection to remove sources with poor astrometric solution is to impose `astrometric_excess_noise < 1` (Lindegren et al. 2018). However, we noticed that Z Cha, for which the *Gaia* parallax ($\varpi = 8.7 \pm 0.1$ mas) implies a distance of 116 ± 2 pc, in good agreement with the distance estimated by Beuermann (2006), 112 ± 8 pc, has `astrometric_excess_noise = 1.08`. Therefore, in order to build a sample that is the most complete as possible, we applied a more generous cut, considering the parallaxes of those sources for which `astrometric_excess_noise > 2` as unreliable.

[1]For example, QZ Lib, one of the few period bouncers known, is located at a distance of 187 pc ($\varpi = 5.3 \pm 0.3$ mas) and is as bright as $G = 18.9$ mag (Pala et al. 2018).

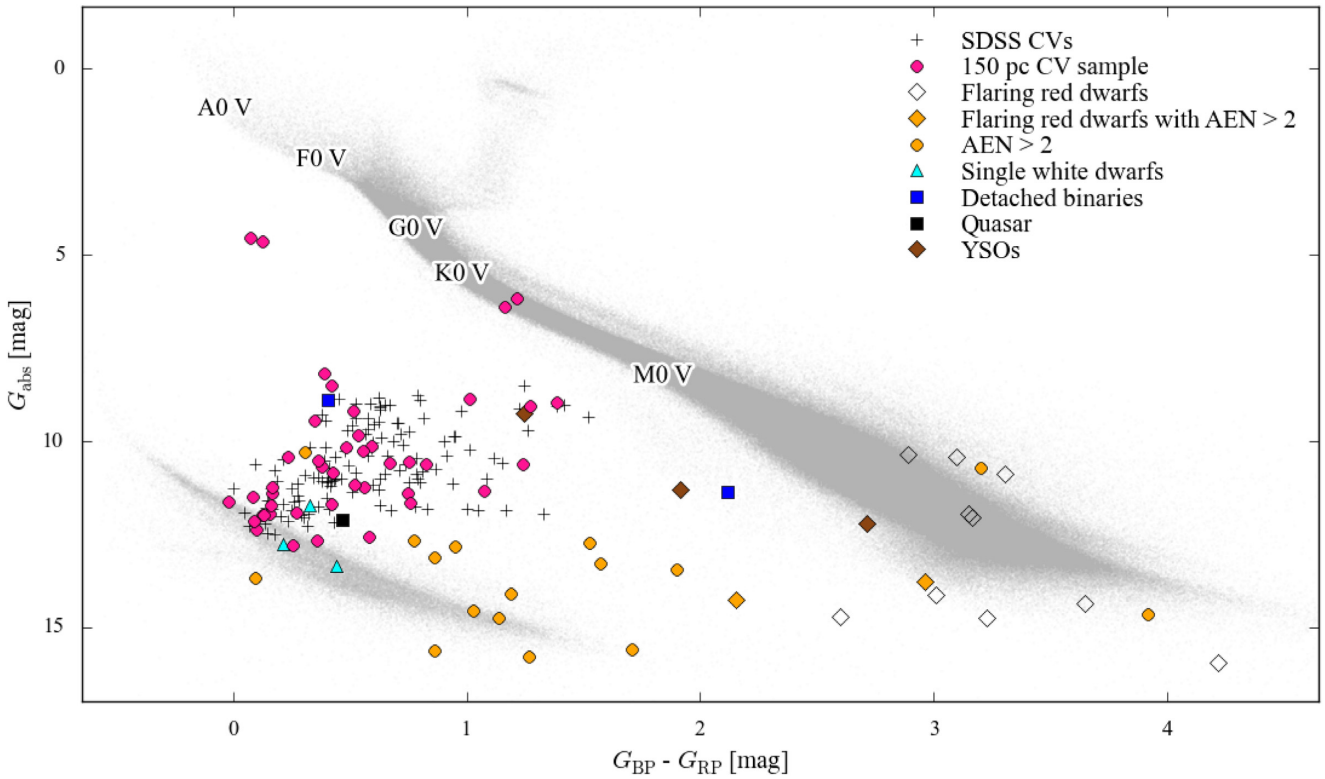

Figure 1. Hertzsprung–Russell diagram of the *Gaia* sources with reliable astrometry (equation 4) located within 150 pc (grey), showing the position of the 150 pc CVs (pink dots, Section 3) and of the different types of contaminants (Section 2) that have been mistakenly identified as CVs or CV candidates within the literature (Appendices A, B, and C). For comparison, SDSS CVs with accurate and clean SDSS photometry (as defined in Section 4) are shown by the black crosses; however, the majority of these systems are at distances $d > 150$ pc. Systems discarded for having high astrometric excess noise (AEN) in *Gaia* are shown in yellow.

2.2 Spurious *Gaia* detections

Ten CV candidates are located in crowded regions and the cross-match between our sample and the *Gaia* catalogue returned a spurious detection (Fig. 3). These sources are actually fainter than the *Gaia* detection limit and do not have an entry in the *Gaia* DR2 archive. Our list also contained EU Cnc for which *Gaia* DR2 provides a parallax of $\varpi = 1.8 \pm 2.5$ mas and therefore satisfies the condition in Equation (1). However, this CV is located in an open cluster for which the distance has been determined as $d = 785 \pm 50$ pc (Belloni, Verbunt & Schmitt 1993) and hence we discarded this system.

3 THE 150 PC CV SAMPLE

Gaia DR2 provided parallaxes for about 1.3 billion sources. Converting these measurements into distances is not always trivial as the mere inversion of the parallax can introduce some biases in the distance estimate, especially when the fractional error on the parallax is larger than 20 per cent (see e.g. Bailer-Jones 2015; Luri et al. 2018). This is the case for many systems in our sample, in particular for those that are further away and have poor parallax measurements. Therefore, to estimate the distances, we used a statistical approach in which, following the prescription by Bailer-Jones (2015), we defined a likelihood and an exponentially decreasing volume density prior. The latter contains the Galactic CV scale height, h, which is a function of the system age: older CVs (i.e. period bouncers and short-period systems that have not evolved through the period minimum yet, $P_{orb} \lesssim 2$ h) have larger scale heights, $h \simeq 260$–450 pc, while younger CVs (i.e. long-period systems, $P_{orb} \gtrsim 2$ h) have smaller scale heights, $h \simeq 120$ pc (Pretorius et al. 2007b). For the systems with a measured orbital period, we defined the relative scale heights following Pretorius et al. (2007b):

$$h = \begin{cases} 120 \text{ pc}, & \text{for long-period systems } (P_{orb} \gtrsim 2 \text{ h}), \\ 260 \text{ pc}, & \text{for short-period systems } (P_{orb} \lesssim 2 \text{ h}), \\ 450 \text{ pc}, & \text{for period bouncer CVs.} \end{cases} \quad (2)$$

Our sample contains three period bouncer candidates, GD 552 (Unda-Sanzana et al. 2008), SDSS J102905.21+485515.2 (Thorstensen, Alper & Weil 2016), and 1RXS J105010.3−140431 (Patterson 2011; Pala et al. 2017), for which we assumed a scale height of $h = 450$ pc. An orbital period determination is not available for *Gaia* J154008.28−392917.6. Nonetheless, its spectral appearances suggest that this is a low accretion rate system of the WZ Sge subtype. These CVs are found below the period gap ($P_{orb} \lesssim 2$ h); thus, for *Gaia* J154008.28−392917.6, we assumed a scale height of $h = 260$ pc.

We determined the distance as the median and the corresponding uncertainties as the 16th and 84th percentiles of the posterior distribution of each system. From the posterior distribution, we also determined the probability for each object to be located within 150 pc. According to these distances, we discarded 55 systems (Table D2) for which $d > 150$ pc.

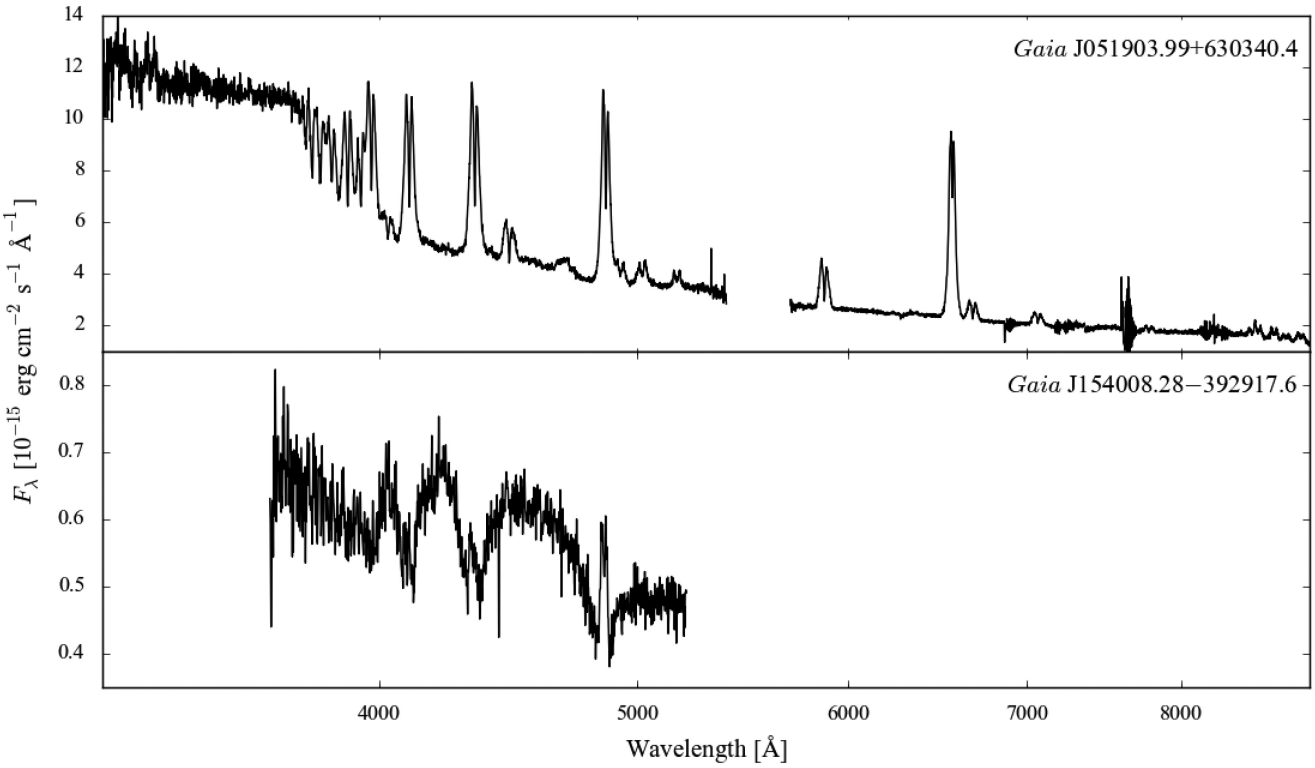

Figure 2. Identification spectra of the two new CVs we discovered within 150 pc. *Gaia* J051903.99+630340.4 (top) presents the typical spectral appearance of an SU UMa CV as it is also confirmed by its orbital period, $P_{\rm orb} \simeq 126$ min (Appendix C), which locates it below the period gap. Dwarf nova outbursts of this system have been detected by ASAS-SN in February 2012, March 2016, and September 2018, during which the system brightened, on average, by $\simeq$5.9 mag. However, in the ASAS-SN observations, the CV is blended with a bright ($V = 10.1$ mag) nearby companion (within $\simeq$7 arcsec, see Section 7). Consequently, during each dwarf nova outburst, only a variation of $\simeq$0.6 mag is observed in the overall brightness recorded by ASAS-SN of the two stars blended together, thus preventing an earlier detection of *Gaia* J051903.99+630340.4 as a CV. Conversely, *Gaia* J154008.28−392917.6 (bottom) is a low accretion rate system of the WZ Sge type, likely located at the period minimum (note its similarity with EZ Lyn in Fig. 8), which has never been observed in outburst so far.

The final 150 pc sample (Table 1) consists of 42 CVs and two AM CVn systems[2] (GP Com and V396 Hya). Although there are many similarities between AM CVn stars and CVs, the formation channels and evolutionary histories of these two classes of systems are different and we do not include the two AM CVn systems in the following discussion (see Ramsay et al. 2018, for a detailed study of these stars using the *Gaia* DR2 data).

Fig. 4 show the spatial distribution of this sample and it is colour coded according to the CV type. The systems appear to be uniformly distributed on the sky, with no evident correlation between their location and their subtypes. In order to evaluate whether the position of the 150 pc CVs on the sky is consistent with a uniform distribution from a statistical point of view, we generated 1000 samples, each consisting of 10^5 objects uniformly distributed in a volume enclosed within 150 pc, assuming an exponentially decreasing space density (Equation 5) with $h = 280$ pc, i.e. the average value of the scale heights of different CV subtypes (Equation 2). For each sample, we randomly selected 42 objects and applied a two-sample Kolmogorov–Smirnov (KS) test between the pairwise cumulative distributions of these objects and that of the CVs in the 150 pc sample. We found that the average KS statistics is $D \simeq 0.03$, lower than the 95 per cent critical level, $D_{\rm critic} \simeq 0.29$, with a *p-value* $\simeq$ 0.7. This implies that the null hypothesis, i.e. uniform distribution on the sky, cannot be rejected, thus suggesting that the 150 pc sample is not affected by obvious selection biases.

4 COMPLETENESS

A key property of any sample used to determine a space density is its *completeness*, in combination with a good understanding of potential observational selection effects. We use two independent tests to assess the completeness of the 150 pc CV sample.

4.1 Previously known CVs with distances

A simple assessment of the completeness of the 150 pc CV sample is to establish the fraction of known CVs with *reliable* pre-*Gaia* distance measurements of $d \leq 150$ pc recovered by *Gaia*. Except parallaxes, all distance measurements are indirect, and we briefly review the main methods used for CVs to qualify what we consider as reliable distances.[3]

[2] An AM CVn system consists of a white dwarf accreting from another white dwarf or a partially degenerate helium star, often via an accretion disc. Their orbital periods are shorter than those of CVs and their optical spectra do not contain any hydrogen.

[3] Ak et al. (2007) proposed a period–luminosity–colour relation, i.e. an alternative empirical calibration in which the absolute magnitude of the system is determined from its period and its 2MASS (Two Micron All Sky Survey, Skrutskie et al. 2006) colours. However, its application to short-period dwarf novae appeared to be problematic (Patterson 2011) and we excluded the distances derived with this method from the following analysis.

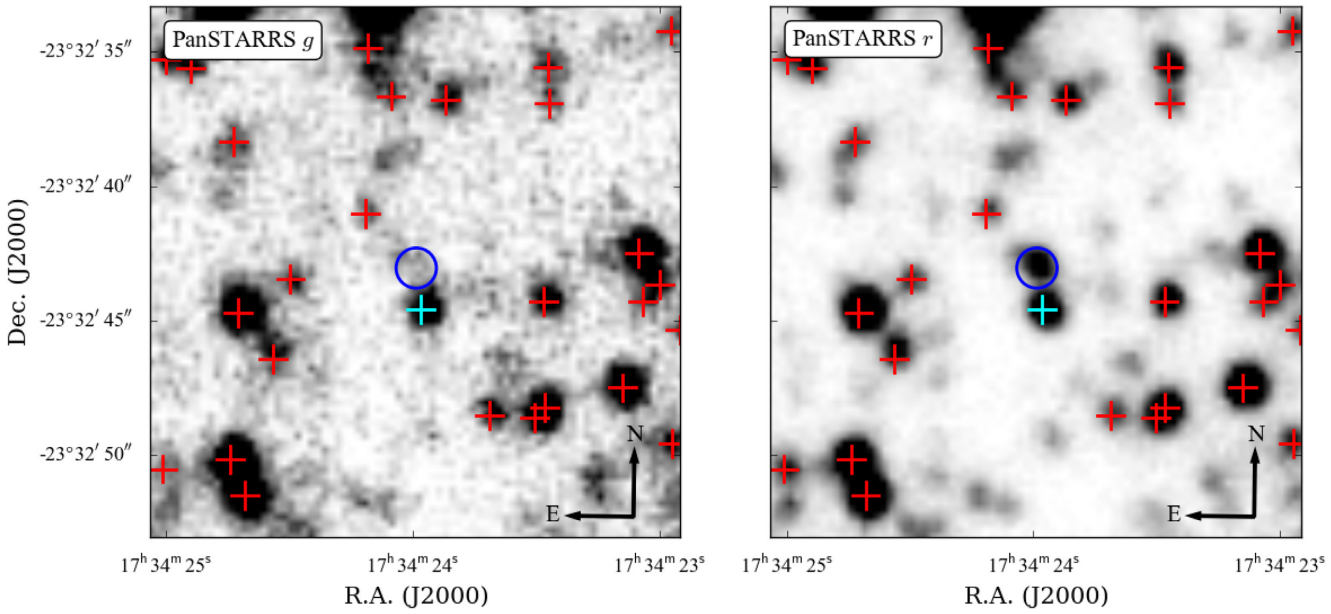

Figure 3. PanSTARRS *g*-band (left) and *r*-band (right) images of OGLE-BLG-DN-0040. The position of OGLE-BLG-DN-0040 is highlighted with a blue circle, while the crosses show the *Gaia* detections, one of which (cyan cross) is located only ≃1.4 arcsec away from OGLE-BLG-DN-0040. However, OGLE-BLG-DN-0040 is fainter than the *Gaia* detection limit in quiescence, so does not have an entry in the *Gaia* DR2 archive. This is actually a spurious association, as can be clearly seen in the *r*-band image.

(a) Accurate trigonometric parallaxes from both space- (Duerbeck 1999; Harrison et al. 2004) and ground-based observations (Thorstensen 2003; Thorstensen, Lépine & Shara 2008).

(b) Modelling the ultraviolet flux of the white dwarf. This method requires a clean detection of the white dwarf that, owing to the strong contamination from the accretion disc in the optical, is best detected in the ultraviolet. By performing a fit to the spectroscopic data, the distance to the system can be measured by assuming a mass–radius relationship, since the scaling factor between the best-fitting model is related to the ratio between the distance and the stellar radius (e.g. Gänsicke et al. 1999).

(c) Modelling the red/infrared photometric contribution of the donor. The emitting area of the secondary is constrained by the Roche geometry, i.e. by the orbital period and the mass ratio. When the secondary is detected in the near-infrared, the distance to the system can be estimated using the 'Bailey method' (Bailey 1981) from its *K* magnitude in combination with the mass–radius relationship for CV secondary stars (e.g. Knigge et al. 2011).

(d) Analysis of the eclipse light curves. Similarly to the modelling of the spectral energy distribution (SED), this method provides both the effective temperature and the radius of the white dwarf, allowing to estimate the distance to the system (Littlefair et al. 2008; McAllister et al. 2019).

(e) M_V–$P_{\rm orb}$ relationship. The radius of the accretion disc is a relatively fixed fraction of that of the white dwarf Roche lobe ($R_{\rm disc} \simeq 0.7 R_{\rm Roche\ lobe}$; Sulkanen, Brasure & Patterson 1981), and scales with the mass ratio and the orbital separation, i.e. with $P_{\rm orb}$. This, combined with the fact that disc outbursts occur when the accretion disc effective temperature rises to ≃8000 K, allows the use of dwarf nova outbursts as standard candles. This method was first introduced by Warner (1987) and later refined by Patterson (2011) using a sample of 46 CVs with good distance estimates. One of the main sources of uncertainty is the often unknown inclination of the system.

We identified 49 CVs with published pre-*Gaia* distance measurements of $d \leq 150$ pc (Table D3). For systems with multiple distance estimates, we considered the most reliable measurement following the order of the list above. *Gaia* re-identified all these 49 CVs, confirming that 28 of them are located within 150 pc. The remaining 21 CVs are found to be located further than their pre-*Gaia* distances, the majority of which were estimated by modelling the red/infrared photometric contribution of the donor. This method systematically underestimates the distance to the systems (Fig. 5) owing to an unaccounted contamination by light from the accretion disc, which results in an overestimate of the brightness of the donor. In contrast, the distances estimated from the modelling of the SED in the ultraviolet are more accurate since the white dwarf is the dominant source of emission in this wavelength range.

Since *Gaia* re-identified all the previously known CVs located within 150 pc, we conclude that the completeness of our sample is not limited by the ability of *Gaia* in obtaining astrometry of CVs but rather by the efficiency of the methods available to identify CVs in the first place. As discussed in Section 2, the discovery of CVs has been strongly biased towards highly variable systems, such as dwarf novae with a high duty cycle, and disfavoured the discovery of systems with both low mass transfer rates (WZ Sge dwarf novae, which have outburst recurrence times of the order of decades) and high mass transfer rates (novalike CVs in which the disc remains in a hot state).

Discovering >300 new CVs, SDSS has demonstrated that the spectroscopic identification of CVs is largely independent of CV subtype. In fact, follow-up of the SDSS CVs led to the unambiguous confirmation of a pile-up of intrinsically faint CVs near the period minimum (Gänsicke et al. 2009). The SDSS CVs represent the currently least biased sample of CVs, and we make use of the *ugriz* photometry to (i) estimate the completeness of our *Gaia* CV sample and (ii) search for CVs within 150 pc that have so far been missed.

Table 1. 150 pc CV sample from *Gaia* DR2, sorted by increasing distance. The CV types are as follows: UG, dwarf nova of U Gem subtype; UGSU, dwarf nova of SU UMa subtype; UGWZ, dwarf nova of WZ Sge subtype; IP, intermediate polar; AM, polar; NL, novalike; AM CVn, AM CVn star. SDSS *ugriz* photometry of the systems highlighted with an asterisk is used to assess the completeness of the *Gaia* 150 pc sample (see Section 4.2).

System	*Gaia* DR2 ID	ϖ (mas)	σ_ϖ (mas)	$P_{\rm orb}$ (min)	Type	G (mag)	$G_{\rm BP}$ (mag)	$G_{\rm RP}$ (mag)	Distance (pc)
WZ Sge	1809844934461976832	22.16	0.04	81.63	UGWZ	15.21	15.21	15.06	45.13 ± 0.08
VW Hyi	4653893040002306432	18.53	0.02	106.95	UGSU	13.84	13.94	13.45	53.96 ± 0.06
EX Hya	6185040879503491584	17.56	0.04	98.26	IP	13.21	13.23	12.88	56.9 ± 0.1
GP Com	3938156295111047680	13.73	0.06	46.57	AM CVn	15.95	15.89	15.91	72.8 ± 0.3
V455 And	1920126431748251776	13.24	0.06	81.08	IP	16.06	16.13	15.71	75.5 ± 0.3
GD 552	2208124536065383424	12.35	0.05	102.73	UGWZ	16.46	16.46	16.18	81.0 ± 0.3
ASASSN-14dx*	2488974302977323008	12.34	0.04	82.81	UGWZ	14.96	14.92	14.69	81.0 ± 0.3
AM Her	2123837555230207744	11.40	0.02	185.65	AM	13.58	13.86	12.85	87.8 ± 0.1
IX Vel	5515820034889610112	11.04	0.03	279.25	NL	9.32	9.34	9.27	90.6 ± 0.2
OY Car	5242787486412627072	11.01	0.03	90.89	UGSU	15.62	15.64	15.21	90.8 ± 0.2
AE Aqr	4226332451596335616	10.97	0.06	592.78	IP	10.95	11.47	10.26	91.2 ± 0.5
U Gem	674214551557961984	10.71	0.03	254.74	UG	13.91	14.38	13.11	93.4 ± 0.3
V396 Hya	3503987633230546688	10.69	0.15	65.10	AM CVn	17.66	17.70	17.45	94 ± 1
BW Scl	2307289214897332480	10.60	0.10	78.23	UGWZ	16.26	16.26	16.10	94.4 ± 0.9
V627 Peg	1800384942558699008	10.03	0.07	78.51	UGWZ	15.67	15.65	15.27	99.7 ± 0.7
AR UMa	783921244796958208	9.87	0.12	115.92	AM	16.26	16.35	15.78	101 ± 1
1RXS J105010.3−140431	3750072904055666176	9.14	0.11	88.56	UGWZ	17.17	17.21	17.08	109 ± 1
TCP J21040470+4631129	2163612727665972096	9.13	0.12	77.07[a]	UGWZ	17.77	17.87	17.29	109 ± 2
V2051 Oph	4111991385628196224	8.90	0.07	89.90	UGSU	15.37	15.46	14.87	112.4 ± 0.9
V834 Cen	6096905573613586944	8.90	0.21	101.52	AM	16.66	16.82	16.07	113 ± 3
GW Lib	6226943645600487552	8.87	0.08	76.78	UGWZ	16.49	16.49	16.32	113 ± 1
ST LMi	3996419759863758592	8.83	0.08	113.89	AM	16.13	–	–	113 ± 1
SS Cyg	1972957892448494592	8.72	0.05	396.19	UG	11.69	12.11	10.95	114.6 ± 0.6
V884 Her	4503256687122329088	8.69	0.02	113.01	AM	13.49	13.57	13.18	115.1 ± 0.3
Z Cha	5210507882302442368	8.66	0.12	107.28	UGSU	15.85	15.94	15.19	116 ± 2
Gaia J051903.99+630340.4	285957277597658240	8.59	0.04	126:	UGSU	15.17	15.30	14.77	116.4 ± 0.5
V2301 Oph	4476137370261520000	8.24	0.08	112.97	AM	16.75	16.94	15.86	121 ± 1
V893 Sco	6039131391540808832	8.06	0.05	109.38	UGSU	14.65	14.76	14.25	124.1 ± 0.8
QZ Vir*	3800596876396315648	7.81	0.07	84.70	UGSU	16.06	16.12	15.76	128 ± 1
V1040 Cen	5343601913741261312	7.80	0.03	87.11	UGSU	14.04	14.11	13.69	128.1 ± 0.4
SDSS J125044.42+154957.3	3934459045528378368	7.79	0.18	86.3	AM	18.22	18.30	17.95	129 ± 3
V379 Tel	6658737220627065984	7.65	0.07	101.03	AM	16.19	16.69	15.45	131 ± 1
BL Hyi	4697621824327141248	7.65	0.07	113.64	AM	17.25	17.45	16.70	131 ± 1
MR Ser*	1203639265875666304	7.59	0.05	113.47	AM	16.23	16.47	15.64	131.8 ± 0.8
V3885 Sgr	6688624794231054976	7.54	0.08	298.31	NL	10.25	10.28	10.16	133 ± 1
Gaia J154008.28−392917.6	6008982469163902464	7.49	0.11	–	UGWZ	17.36	17.39	17.23	134 ± 2
VV Pup	5719598950133755392	7.30	0.05	100.44	AM	15.93	16.04	15.48	137.0 ± 0.9
VY Aqr	6896767366186700416	7.24	0.14	90.85	UGSU	16.86	16.96	16.44	138 ± 3
IP Peg	2824150286583562496	7.08	0.05	227.82	UG	14.71	15.27	13.88	141.2 ± 1.0
HT Cas	426306363477869696	7.07	0.06	106.05	UGSU	16.35	16.48	15.81	141 ± 1
SDSS J102905.21+485515.2	834947865750806272	6.96	0.24	91.33	UGWZ	18.16	17.94	17.84	144 ± 5
EZ Lyn*	935056333580267392	6.87	0.15	84.97	UGWZ	17.81	17.84	17.71	146 ± 3
V379 Vir*	3699606286708406912	6.7	0.2	88.4	AM	18.01	18.02	17.93	150 ± 4
V355 UMa	1558322303741820928	6.66	0.09	82.52	UGWZ	17.38	17.35	17.27	150 ± 2

[a]Spectroscopic period (ATel #13009).

4.2 Completeness of the 150 pc CV sample

Because the majority of known CVs fall within the colour space of quasars, we can make use of the highly efficient spectroscopic follow-up of SDSS quasar candidates to assess the completeness of the 150 pc CV sample. The uniform spatial distribution of the 150 pc CVs (Section 3) suggests that the properties of the local CV population are not evidently correlated with their location on the sky and that CVs are identified with equal success at low and high Galactic latitudes. Moreover, the typical CV scale height (h = 280 pc) is much larger than the radius (h = 150 pc) of the volume we are considering, and consequently, the correlation of the distribution of the 150 pc CVs with the Galactic latitude is negligible. For this reason, although the SDSS footprint covers only one-third of the sky and avoids the Galactic plane, the properties of the SDSS CVs can be safely extended to the whole sky and hence to the 150 pc *Gaia* CV sample.

4.2.1 Definition of the spatial and colour footprint followed up by the SDSS quasar search

With the aim to study extragalactic objects, SDSS acquired photometric observations for 7500 deg^2 of sky and subsequently performed spectroscopic follow-up for a subset of the photometric objects. SDSS selected the spectroscopic quasar targets according to their colours (Richards et al. 2002). Within the vicinity of a quasar in the four-dimensional ($u-g$; $g-r$; $r-i$; $i-z$) colour

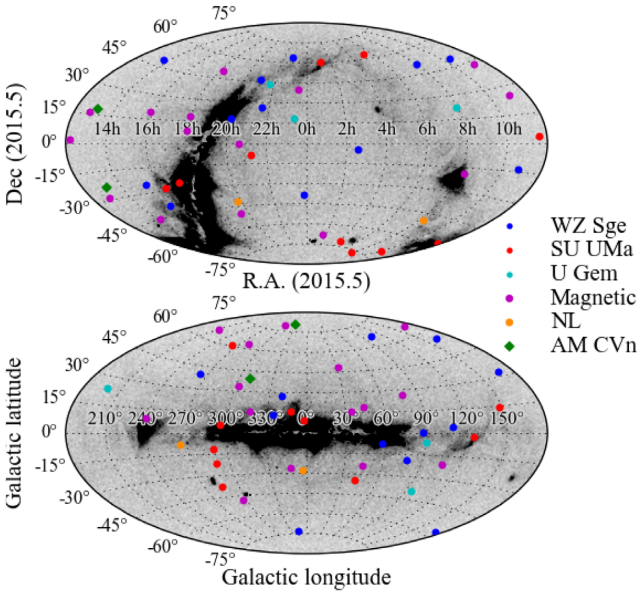

Figure 4. The spatial distribution of CVs in the 150 pc sample in equatorial (top) and Galactic (bottom) coordinates shows no evident correlation with the different subtypes, suggesting that the 150 pc CV sample is not affected by obvious selection biases.

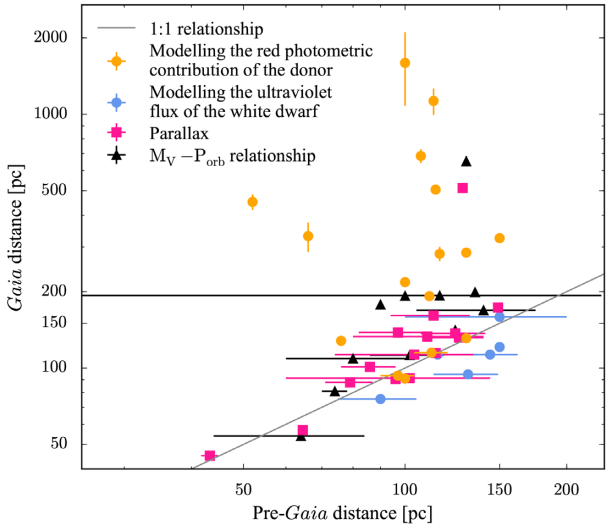

Figure 5. Comparison between pre-*Gaia* distances estimated using different methods and distances based on the *Gaia* parallaxes. The most accurate pre-*Gaia* distances have been determined from ground- and space-based parallax measurements (pink). Whereas modelling ultraviolet spectra of white dwarf dominated CVs (blue) also provides reliable distance measurements, estimates based on modelling the red/infrared photometric contribution of the donor stars (orange) systematically overestimate the distance. Although subject to large uncertainties, the distance estimates from the M_V–P_{orb} relationship are consistent with the *Gaia* determinations for most of the systems in the sample.

space, all photometric objects have the same probability to be spectroscopically observed by the Legacy (York et al. 2000) and BOSS (Baryon Oscillation Spectroscopic Survey; Dawson et al. 2013).

Consequently, the probability for an object to be observed spectroscopically depends on its location on the sky (i.e. whether it is located within the Legacy/BOSS footprint) and on its colour similarity to quasars. To define this parameter space, we used the CasJobs[4] service to query the PlateX table imposing `programName == 'boss' || programName == 'legacy'`. This returned the coordinates of the centres of the 4235 spectroscopic plates observed by the Legacy and BOSS. Each spectroscopic plate has a field of view of 1.49° in radius; therefore, objects located within ≤1.49° from the plate centre that have (i) fibre magnitudes, i.e. the flux contained within the aperture of a spectroscopic fibre, fainter than 15 mag in g or r, and 14.5 mag in i, and (ii) $i < 19.1$ mag are all potential spectroscopic targets. These magnitude limits are imposed by the fixed 15 min exposure time of the SDSS observing strategy: objects brighter than the first set of limits saturate the SDSS detectors and objects fainter than $i = 19.1$ are so numerous that they were not systematically followed up spectroscopically. We used the quasar catalogue from the SDSS DR7 (Schneider et al. 2010) to calculate the colour distance, i.e. the nearest-neighbour distance, between each pair of quasars. We found that ≈99 per cent of them have another quasar within ≃0.29 mag. We can hence assume that all objects found within 0.29 mag from a quasar are located within the colour space in which SDSS selected its spectroscopic targets and had therefore a chance to be observed spectroscopically.

CVs occupy a subregion of the colour space in in which quasars are found. This subregion can be defined in an analogous fashion as done above for the case of quasars. We calculated the colours ($u - g$; $g - r$; $r - i$; $i - z$) of all known CVs with SDSS photometry. To avoid contamination from objects with poor photometry or objects mistakenly classified as CVs, we only considered SDSS sources that could be matched to CVs that were confirmed either by spectroscopy or by a published orbital period measurement, and that have accurate (photometric errors < 5 per cent) and clean SDSS photometry, i.e.

```
clean = 1 & mode = 1 & type = 6.        (3)
```

These flags ensure selection of stars (`type = 6`) rather than galaxies and avoid blended photometry or multiple detections of the same source. We also required that the selected objects have reliable *Gaia* parallax and colours (Equation 4). The final sample contains high-quality photometry of 418 CVs, the majority of which are located further than 150 pc. In order to build a reference CV sample that is as representative as possible of the overall SDSS CV population, we computed the apparent magnitudes that SDSS CVs with $d > 150$ pc would have if they were located at $d = 150$ pc. This allows us to remove those systems that, if they were closer, would have not been observed by SDSS owing to the bright limit in the target selection. Moreover, we only considered those CVs that fulfil the conditions listed above (location on the sky and colour similarity with quasars), which reduced the reference sample to 130 CVs (black crosses in Fig. 1).

We then defined a four-dimensional 'sphere' in colour space, centred on each of these 130 CVs, and calculated the colour distance between each pair. Fig. 6 shows that the distribution peaks at a colour distance of ≃0.06 mag; however, to enclose 95 per cent of the sample, we defined a colour radius of ≃0.27 mag. All objects located within ≤0.27 mag from any of these 130 reference CVs are hence potential CV candidates. From their spectral completeness (i.e. the ratio between the objects with a spectrum and the total number of objects observed photometrically) combined with the fraction of spectroscopically observed objects drawn from that colour space that actually are CVs, one can then estimate how many CVs are

[4] https://skyserver.sdss.org/casjobs/

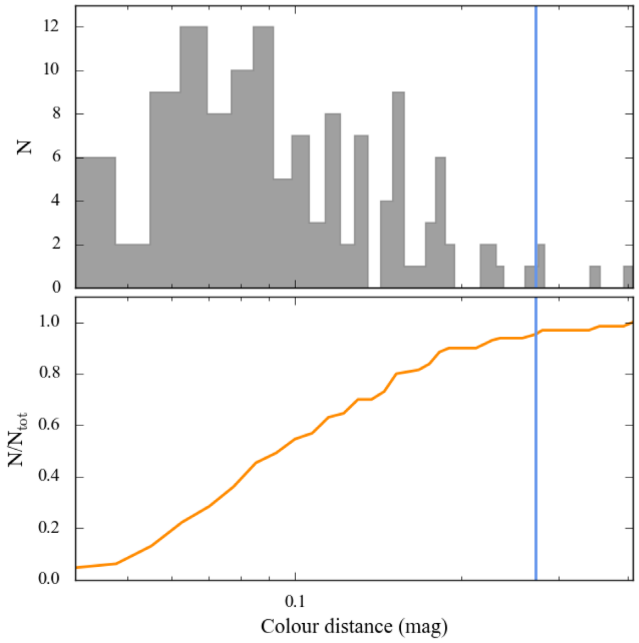

Figure 6. Frequency distribution (top) and cumulative distribution (bottom) of the colour distance in the four-dimensional space ($u-g$; $g-r$; $r-i$; $i-z$) for the 130 SDSS CVs, showing that 95 per cent of them have another CV within ≃0.27 mag (vertical blue line).

expected to be found among the candidates. Comparing the expected number of CVs with that of known CVs within the reference spatial and colour footprint then provides the completeness of the sample. In the following section, we apply this method to the SDSS CVs in order to derive the completeness of the 150 pc *Gaia* CV sample.

4.2.2 *Application to the 150 pc sample*

We performed a cross-match between *Gaia* and SDSS,[5] querying the *Gaia* archive for all objects that, including their parallax uncertainties, are located within 150 pc (Equation 1), which returned ≃2 100 000 objects. Among them, many systems have inaccurate astrometry and $G_{\rm BP}-G_{\rm RP}$ colours due to faintness, blended double stars, or other astrometric effects. Following the prescription from Lindegren et al. (2018, their appendix C), we selected only those sources with the most reliable astrometry by applying the following cuts:

$$\begin{aligned} &\texttt{astrometric\_excess\_noise} < 1,\\ &\texttt{phot\_bp\_rp\_excess\_factor} > 1+0.015\times \texttt{bp\_rp}^2,\\ &\texttt{phot\_bp\_rp\_excess\_factor} < 1.3+0.06\times \texttt{bp\_rp}^2, \end{aligned} \quad (4)$$

which leaves ≃910 000 objects with reliable *Gaia* colours and astrometry (grey dots in Fig. 1).

We then queried the SDSS DR14 archive using the CasJobs website and retrieved the SDSS coordinates, photometry, and Modified Julian Date of the observations for the closest objects within 30 arcsec to each *Gaia* entry. Using the *Gaia* proper motions, we calculated the coordinates of the *Gaia* sources at the epoch of the SDSS observations, and then performed a 2 arcsec radius cross-match with the SDSS objects, thus obtaining the best epoch-matched association between each *Gaia* entry and the SDSS DR14 sample for a total of ≃300 000 objects.

Data releases later than DR7 provide more accurate photometry based on an improved background subtraction. As a side effect of this re-reduction of the photometry, some sources nearby bright stars that were present in DR7 are no longer included in the later data releases. To recover these lost sources, we applied the procedure outlined above also to the SDSS DR7 catalogue, retrieving photometry for an additional ≃4000 sources that are no longer included in the subsequent data releases.

The final cross-match between the *Gaia* source within 150 pc and SDSS contains 303 723 objects (Table 2).

Among these 303 723 objects, 5300 (2811 of which have a spectrum) fall within the spatial and colour footprint of our SDSS CV reference sample defined above and are hence CV candidates (Fig. 7). Four of these are known CVs (V379 Vir, EZ Lyn, MR Ser, ASASSN-14dx), three of which (V379 Vir, EZ Lyn, and MR Ser) have a spectrum (Fig. 8).

The spectra of these 2811 objects were then visually inspected, but no additional CV was identified. This is not surprising given the extensive search for CVs in the SDSS data that has been carried out in the past by Szkody et al. (2002, 2003, 2004, 2005, 2006, 2007, 2009, 2011). The spectral completeness of the CV candidate sample is $2811/5300 \simeq 53$ per cent. Considering that there are three CVs with a spectrum, we can hence estimate that a total of ≈6 CVs were expected to be identified. Since only four CVs have been detected, we can conclude that the sample is ≈ 71 per cent complete (Fig. 9). This estimate of the completeness is subject to small number statistics, and we derive a more robust value making use of the much larger sample of CVs with CRTS light curves.

4.2.3 *Additional constraints from CRTS light curves*

Additional constraints on the completeness can be derived from the long-term light curves of the 2489 CV candidates identified in Section 4.2.1 for which no SDSS spectroscopy is available, which provide the possibility to discover new CVs via the detection of their intrinsic variability. CRTS light curves are the most suitable for this task since, spanning more than 10 yr, they are sensitive to the low mass transfer rate systems with disc outburst recurrence times of years (e.g. Breedt et al. 2014). Moreover, covering ≃30 000 deg^2 of the sky between $-75^\circ < \delta < 65^\circ$ and $|b| \gtrsim 15^\circ$ (Drake et al. 2009), the CRTS footprint largely overlaps with that of SDSS, allowing us to combine the spectral completeness constraints derived in the previous section with the presence of possible variability.

Whereas the CRTS observing strategy aimed at obtaining data with ≃2-week cadence, seasonal visibility and adverse weather condition can result in quite a different number of observations per field, and therefore, the CRTS data for a given object span a wide range in quality. Therefore, it is necessary to define a criterion that identifies intrinsic variability opposed to possible scatter due to poor weather conditions, cosmic ray contamination, and possible calibration issues. To this purpose, we used a sample of 1807 hydrogen-atmosphere white dwarfs from Gentile Fusillo et al. (2019, flagged as 'DA' in their table 4) that are located within 150 pc and have been observed by CRTS, but are not variable (a small number of white dwarfs exhibit variability due to pulsations or rotations, though with amplitudes that are much lower than the variability seen among CVs). Since these systems

[5]While the *Gaia* consortium already provides the cross-match with SDSS (gaiadr2.sdssdr9_best_neighbour), we found that ≃82 000 objects common to SDSS and *Gaia* are missing from that table, as well as ≃1000 associations of spurious *Gaia* data with SDSS sources.

Table 2. Summary of the cross-match between *Gaia* and SDSS and the relative subsamples used to estimate the completeness in Section 4.

Description	Number of objects
Total number of sources in *Gaia* DR2 with $\varpi + 3\sigma_{\varpi} \geq 6.66$ mas	2100 094
Number of sources with reliable astrometry (Equation 4)	910 187
of which in SDSS	303 723
of which in SDSS DR14	299 501
of which in SDSS DR7	4222
of which within the Legacy and BOSS footprint	155 099
of which in the quasar colour space	42 823
of which with similar colour to CVs	5300
of which with a spectrum	2811

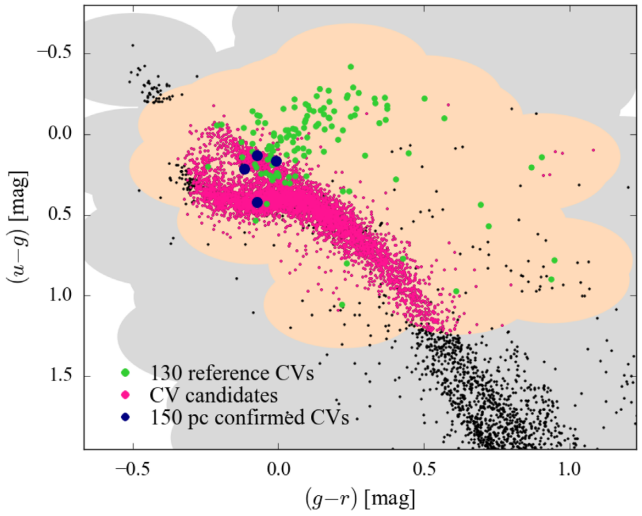

Figure 7. Two-dimensional projection of the four-dimensional ($u - g$; $g - r$; $r - i$; $i - z$) colour space on to ($u - g$; $g - r$) of the sources within 150 pc (black) that are found within the quasar colour space (grey). The four-dimensional colour space spanned by CVs has been defined by 130 reference CVs (green dots, Section 4.2.1), and the projection of that colour space on to ($u - g$; $g - r$) is shown by the light orange cloud. CV candidates contained within this four-dimensional colour space are shown in pink. Among them, four confirmed CVs (dark blue) are known. Given the spectral completeness of $\simeq$53 per cent, $\approx$2 more CVs are expected to be identified, implying an overall completeness of $\approx$ 71 per cent for the 150 pc CV sample.

are not intrinsic variable, in an ideal data set, all data points of a light curve should be consistent with the median value within their uncertainties. Consequently, the related reduced chi-squared χ^2_ν should converge to $\approx$1 as the number of degrees of freedom, $\nu = N - 1$ (where N is the number of observations), increases, whereas the standard deviation of the normalized residuals should be $|\sigma_{\rm RES}| < 2$. We queried the CRTS data base[6] for the light curves of the white dwarf test sample. We considered only observations with $V \geqslant 13$ mag to avoid saturated exposures and computed the χ^2_ν associated with each light curve. We found that χ^2_ν shows a much larger scatter than expected (Fig. 10), reflecting the presence of low-quality photometric observations that mimic the presence of intrinsic variability in the systems. Using those white dwarfs that appear intrinsically variable owing to the low quality of their CRTS observations (Fig. 10, orange and pink points), we defined the following two cuts that remove systems with poor CRTS data:

$$\chi^2_\nu > \frac{300}{\nu} + 3.5 \quad \text{or} \quad |\sigma_{\rm RES}| > 2. \tag{5}$$

Three per cent of the objects satisfy the condition above and this fraction represents the intrinsic systematic uncertainty associated with this selection method.

To verify the quality of our criteria, we applied the same cuts to a control sample of 456 CVs from Drake et al. (2014) for which CRTS light curves having at least three data points[7] with $V \geqslant 13$ mag are available. Our method outlined above is able to identify as variable 93 per cent of these CVs. The 7 per cent of systems that we are unable to recover are those showing low variability or having a low number of observations ($N \lesssim 10$).

We then repeated the same exercise for the 2489 CV candidates without a spectrum (Table 3 and Fig. 11, left branch), since these are the objects for which the lack of additional information prevents us from establishing their true nature. As before, we queried the CRTS data base for unsaturated exposures and we considered only light curves with three or more data points, which were available for 1983 objects.

Applying equation (5), we find that 3.5 per cent of them are variable. This fraction needs to be corrected for the fact that our method is unable to recover seven per cent of the 456 CVs from the control sample from Drake et al. (2014), thus resulting in a total fraction of 10.5 per cent (i.e. 208) variable objects, which are possible CV candidates. These need to be complemented with the remaining 2489 − 1983 = 506 sources for which no information (neither an SDSS spectrum nor a CRTS light curve) is available and that could also hide a not yet identified CV. The total 714 systems, representing 13 per cent of the 5300 candidates identified in the previous section, are the sources for which we are unable to unambiguously establish whether they are CVs and set an upper limit for the completeness of our sample to 87 per cent.

A lower limit on the completeness can be derived imposing more stringent constraints on the CRTS light curve. Ideally, 200 points are in principle sufficient to identify short-term variability (not necessarily related to disc instabilities, such as eclipses) in low-mass accreting short-period systems (Parsons et al. 2013). However, in order to obtain a conservative lower limit on the completeness, we decided to impose a more stringent constraint, assuming that

[6] http://nesssi.cacr.caltech.edu/DataRelease/

[7] Ideally, three data points represent a lower limit for the number of observations required to identify a CV candidate since two observations during quiescence allow to define a quiescent reference level with respect to which any significantly bright (even single) outlier can be indicative of the occurrence of a disc outburst.

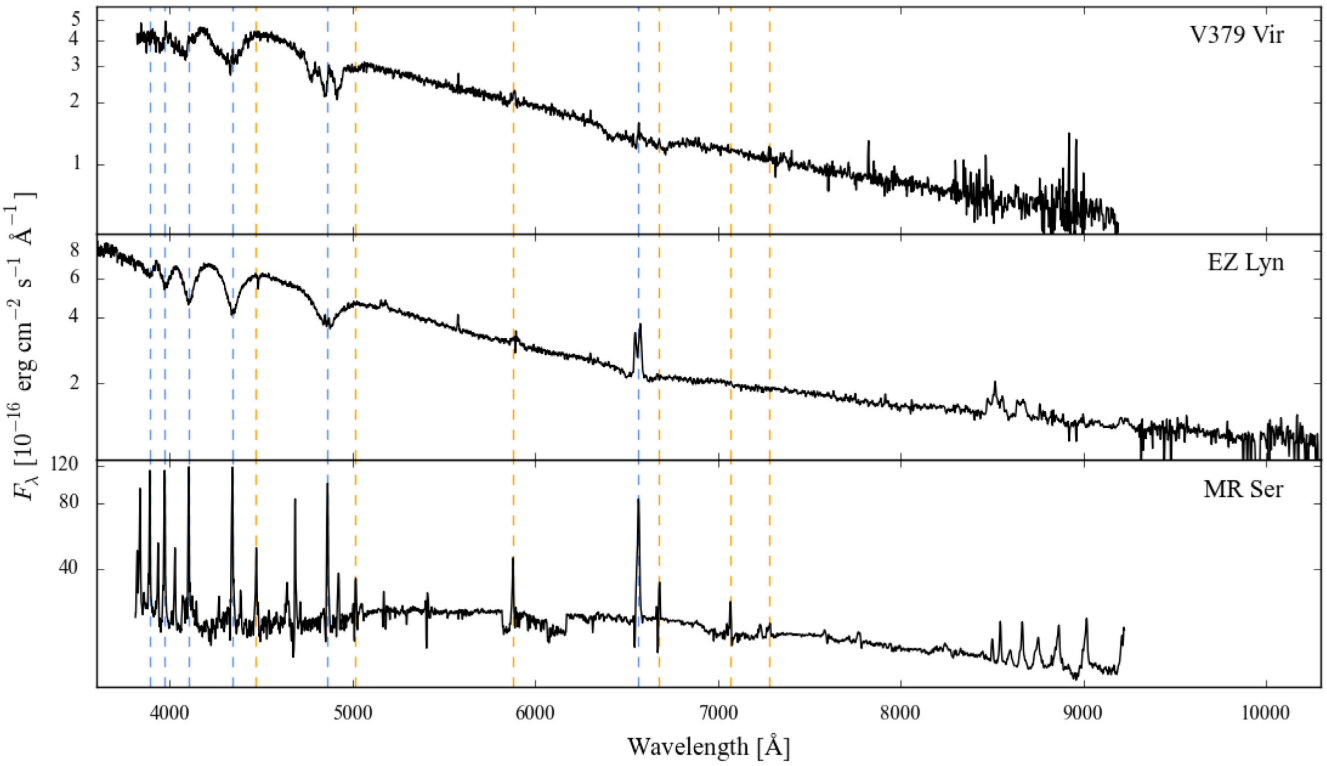

Figure 8. SDSS spectra of the CVs in the 150 pc SDSS sample. The blue and the orange dashed lines highlight the position of the Balmer series and of some of the most common He I lines, respectively. EZ Lyn shows the typical spectral appearance of the low-accreting WZ Sge type CVs, with the white dwarf signature clearly recognizable in the broad Balmer line absorption features. Magnetic CVs undergo phases of high mass transfer (high states) alternated with phases in which accretion almost ceases (low states). Among the magnetic systems in the 150 pc sample observed by SDSS, V379 Vir has been caught in a low state, while MR Ser has been observed in a high state.

a minimum of 300 data points are necessary to identify variable systems. In this case, our control sample is reduced to 71 CVs from Drake et al. (2014) for which CRTS light curves with at least 300 unsaturated exposures are available and, with our selection criteria defined in Equation (5), we are able to recover as variable 97 per cent of them.

Among the 2489 CV candidates without a spectrum, 839 have CRTS light curves matching the new requirement of 300 data points (Table 3 and Fig. 11, right branch) and one per cent of them are variable according to Equation (5). Accounting for the fact that, in this case, our method is unable to recover three per cent of CVs results in a total fraction of four per cent variable objects, i.e. 34. Adding these to the $2489 - 839 = 1650$ objects for which we have no information (neither SDSS spectra nor CRTS light curves) results in a total of 1684 CV candidates. These correspond to 32 per cent of the initial 5300 candidates, implying a lower limit of 68 per cent in the completeness of our sample.

Considering the upper and lower limits derived above, we conclude that our sample is (77 ± 10) per cent complete, where the error is estimated as the sum of the maximum uncertainties in our method (seven and three per cent, respectively), representing the efficiency in recovering CVs as a function of the number of observations available.

4.3 Summary on the completeness

Using two independent methods, i.e. the count of objects with a spectrum (Section 4.2.2) and the count of objects found to be variable (Section 4.2.3), we obtained two values for the completeness, $\approx$ 71 and (77 ± 10) per cent, respectively, that are in good agreement among each other, thus supporting the validity of our result.

Because of the larger sample size of CVs used for the computation of the completeness carried out in Section 4.2.3, we adopt (77 ± 10) per cent as the final value. As stated earlier, the CVs and CV candidates used in this analysis have only been selected according to their position on the sky and colours and hence the completeness estimate can be safely extended to the whole *Gaia* 150 pc CV sample. Given the (77 ± 10) per cent completeness, we can estimate that $\approx$12 CVs are still to be discovered within 150 pc.

The methods we employed to derive the completeness are based on the SDSS quasar target selection, and are biased against red, donor-dominated CVs. Moreover, such systems, if located within 150 pc, are too bright to be selected as spectroscopic targets by SDSS owing to the saturation limit of the SDSS photometry. Nonetheless, it is reasonable to assume that all SU UMa and U Gem CVs within 150 pc have already been identified since their brightening during their relatively frequent outbursts would have unlikely been missed by the many time-domain surveys and amateur observers that regularly scan the sky for transient events (see e.g. Breedt et al. 2014, for a case study of CRTS). An example is U Gem, the prototype for its class, which is known since 1855 (Pogson 1857) and has been been observed photometrically by SDSS, but not spectroscopically owing to its brightness ($g = 14.6$ mag).

Instead, we cannot exclude that some WZ Sge systems, novalike CVs, and polars within 150 pc remain to be identified: ASASSN-14dx, a WZ Sge star located at $d = 81.0 \pm 0.3$ pc with a quiescent magnitude of $V \simeq 16.2$ mag (Thorstensen et al. 2016), and TCP J21040470+4631129, another WZ Sge-type CV located at $d = 109 \pm 2$ pc with a quiescent magnitude of $V \simeq 17.7$ mag

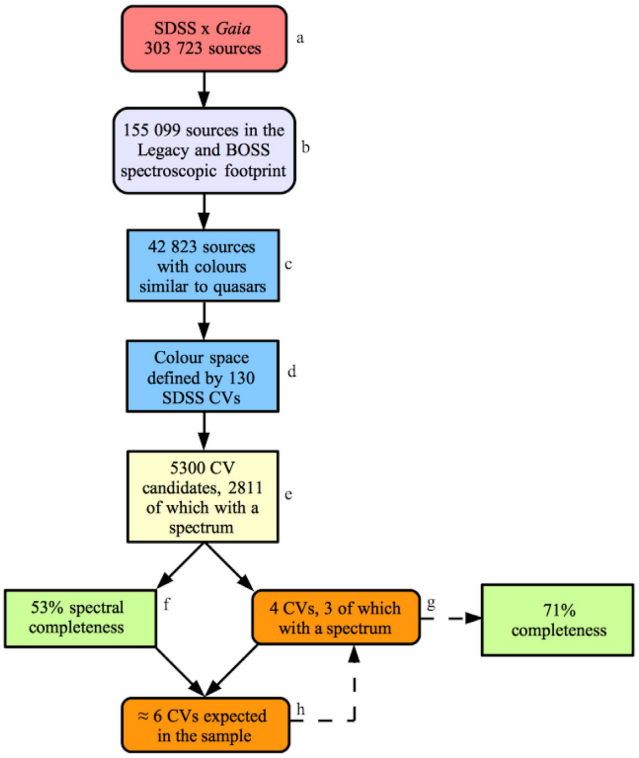

Figure 9. Flowchart of the process used to estimate the completeness of the 150 pc sample. The starting point is the cross-match between *Gaia* and SDSS (a), which returns 303 723 sources. A subsample of these, 155 099 (b), falls within the footprint that the SDSS Legacy and BOSS observed spectroscopically. Among them, 42 823 have colours similar to quasars (c) and hence have all the same probability to have a spectrum in SDSS. Thanks to their colour similarity with the 130 SDSS CVs (d) that occupy a subregion of the quasar colour space (see Section 4.2.1), 5300 CV candidates are identified, 2811 of which have a spectrum (e). This implies a spectral completeness of 53 per cent (f). This sample contains four known CVs, three of which have a spectrum (g). We can hence estimate that ≈6 CVs should be identified in total (h). Four CVs have already been found and we can conclude that the CV sample is ≃71 per cent complete (i).

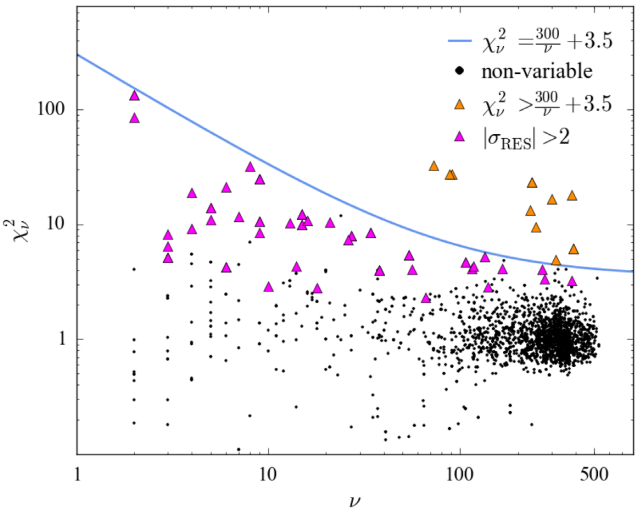

Figure 10. Sample of 1807 hydrogen-atmosphere white dwarfs used to define the criteria for identifying variable systems. Systems above (orange points) or below the threshold (light blue) but with $|\sigma_{\rm RES}| > 2$ (pink dots) are identified as variable.

(ATel #12936), have only been discovered in 2014 and 2019, respectively, following a dwarf nova outburst. We can conclude that the missing systems are most likely those showing low or no variability, such as (i) low mass transfer rate systems with outburst recurrence times of decades; (ii) high mass transfer rate systems (i.e. novalikes) with stable, hot accretion discs; and (iii) strongly magnetic discless systems that do not experience disc outburst, which have been in a low state during the *ROSAT* All-Sky X-ray survey, and other serendipitous X-ray observations.

As a final remark, it is important noticing that the colour footprint in which we searched for CV candidates (Fig. 7) includes the region in which these low-variability systems are expected to be located, and therefore, the methods we used to derive the completeness are optimally accounting for those objects that most likely are still missing in the 150 pc CV sample.

5 SPACE DENSITY

To determine the space density of CVs, we assumed a Galactic model following the prescription of Pretorius et al. (2007a) and approximated the Galaxy as an axisymmetric disc, with no halo, no bulge, no spiral structure, and no thick disc. We assumed the following density profile:

$$\rho = \rho_0 \exp\left(-\frac{|z|}{h}\right), \tag{6}$$

where z is the distance above the Galactic plane, ρ_0 is the space density in the mid-plane, and h is the scale height of the CV population. We ignored any possible dependences from the radial distance from the Galactic centre since they are negligible within the volume we are considering.

ρ_0 is then calculated as the ratio between the number of CVs ($N_{\rm CV}$) found in the effective volume ($V_{\rm eff}$) for a given Galactic model (i.e. for a given scale height) and the effective volume itself. One of the unknowns in the determination of the space density is the scale height of the CV population. As discussed in Section 3, h depends on the age of the population, and with the small number of CVs within 150 pc, it is not possible to independently measure h. We therefore assumed $h = 100$, 280, and 500 pc and determined ρ_0 using a Monte Carlo approach to evaluate the effective volume enclosed within a given distance (middle panel of Fig. 12). For our distance limit of 150 pc, we found a variation of ≃30 per cent of ρ_0 for the two extreme cases of h (≃4.8×10^{-6} pc^{-3} for $h = 100$ pc and ≃3.4×10^{-6} pc^{-3} for $h = 500$ pc, respectively; see Table 4). However, the 150 pc CV sample is dominated by old CVs and hence the higher values we assumed for h are more likely to be more representative of the properties of the observed sample.

In order to investigate for the presence of possible biases as a function of distance, we divided the 150 pc volume in four bins of equal volume (bottom panel of Fig. 12). Within the uncertainties ρ_0 remains constant in the four bins, although its value decreases in the outer bin, reflecting the presence of possible detection biases. However, the cumulative distributions of the different CV subtypes (Fig. 13) all show the same trend suggesting that, whether present, these detection biases affect all CV subclasses in the same way.

Considering the volume enclosed within 150 pc, and accounting for the Poisson uncertainties, a conservative measurement of the space density of known CVs gives $\rho_0 = (3.7^{+0.6}_{-0.8}) \times 10^{-6}$ pc^{-3} for $h = 280$ pc (solid line in the middle panel of Fig. 12). The related 3σ uncertainties (dotted lines in the middle panel of Fig. 12) also include the uncertainty due to the unknown scale height of the Galactic CV population. Accounting for the possibility that the

Table 3. Summary of the different subsamples used to estimate the completeness from CRTS light curves (Section 4.2.3).

Description	Number of objects
Source with colour similarity to CVs	5300
of which without a spectrum	2489
of which with a CRTS light curve with more than three unsaturated data points	1983
of which variable	208
of which without a CRTS light curve with more than three unsaturated data points	506
of which with a CRTS light curve with more than 300 unsaturated data points	839
of which variable	34
of which without a CRTS light curve with more than 300 unsaturated data points	1650

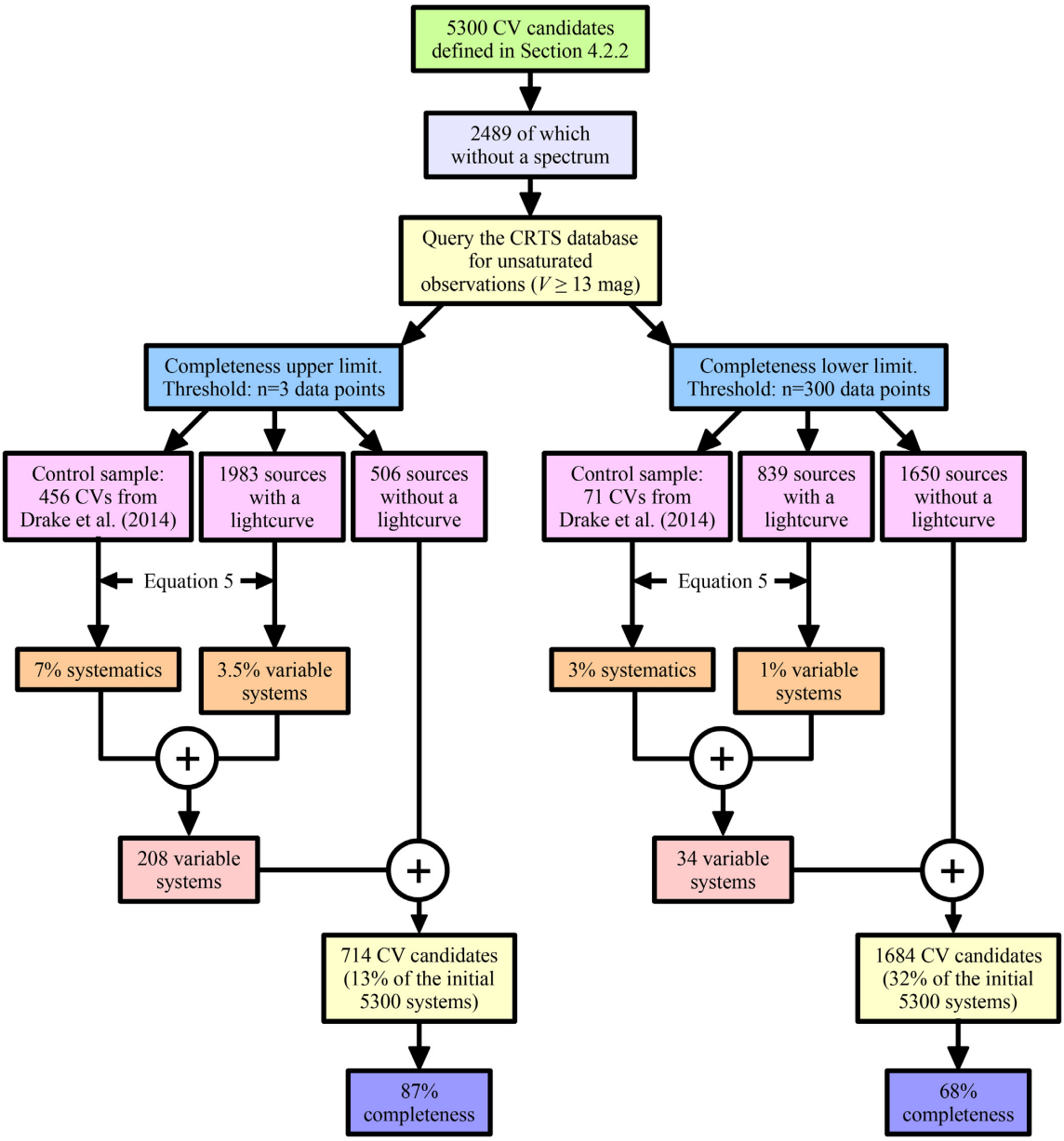

Figure 11. Flowchart of the process used to estimate the completeness of the 150 pc sample using CRTS. The starting point is the 5300 CV candidates identified in Section 4.2.2. 2489 of them do not have a spectrum and thus lack additional information required to establish their true nature. Using their CRTS light curves, we establish the number of objects for which we are unable to unambiguously establish whether they are CVs, thus obtaining an upper and a lower limit for the completeness of the 150 pc CV sample.

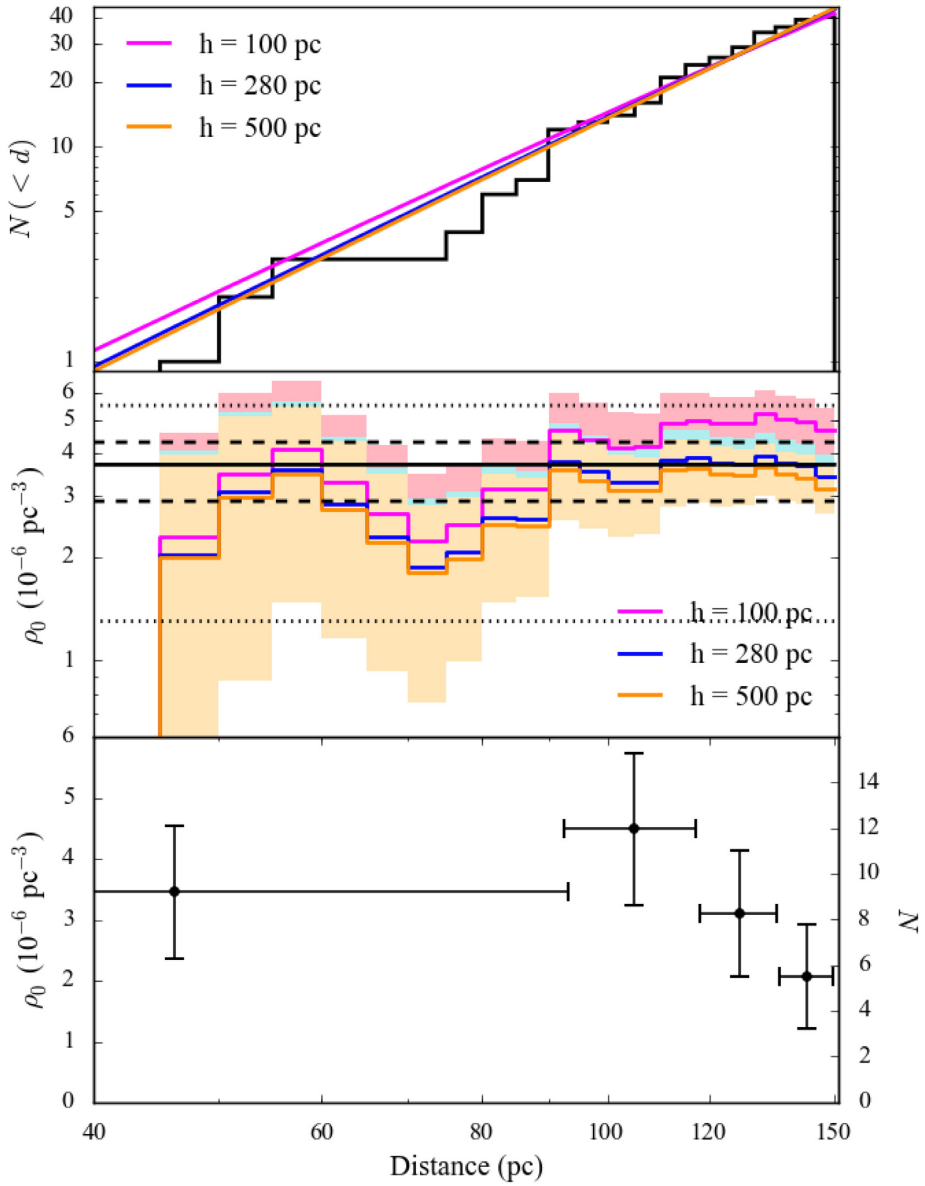

Figure 12. Top: Cumulative distribution of the 150 pc CV sample as a function of the distance (black line) in comparison with the prediction by the Galactic model assuming different scale heights (coloured lines as indicated). Middle: ρ_0 as a function of distance for different scale heights. The black solid line corresponds to our conservative value of the CV space density $\rho_0 = (3.7^{+0.6}_{-0.8}) \times 10^{-6}$ pc^{-3} for $h = 280$ pc. The dashed and dotted lines represent the relative 1σ and 3σ uncertainties, respectively. Bottom: CV space density in four bins of equal volumes. The error bars report the Poissonian uncertainties.

Table 4. CV space densities for different scale heights. Both the values and the number of systems (N_{CV}) derived from the analysis of the *Gaia* data and the corresponding ones corrected for the completeness of the sample are reported.

h (pc) \ d_{lim} (pc)	150	
Completeness	77%	100%
N_{CV}	42	54
	ρ_0 [10^{-6} pc^{-3}]	
100	$4.8^{+0.8}_{-1.0}$	$6.3^{+0.9}_{-1.1}$
280	$3.7^{+0.6}_{-0.8}$	$4.8^{+0.6}_{-0.8}$
500	$3.4^{+0.5}_{-0.6}$	$4.3^{+0.5}_{-0.7}$

Gaia CV sample is only 77 per cent complete would imply a space density of $\rho_0 = (4.8^{+0.6}_{-0.8}) \times 10^{-6}$ pc^{-3} for $h = 280$ pc, which would still be consistent with the conservative value derived above without introducing any correction for incompleteness.

Prior to our *Gaia*-based analysis, the most reliable space density had been estimated using an X-ray selected sample of CVs, $\rho_0 = 4^{+6}_{-2} \times 10^{-6}$ pc^{-3} (Pretorius & Knigge 2012). Schwope (2018) recently revisited this sample, making use of the *Gaia* distances, and derived $\rho_0 < 5.1 \times 10^{-6}$ pc^{-3}. Both studies assumed that this magnitude-limited sample of X-ray selected CVs is complete and representative of the intrinsic population, leaving systematic uncertainties of a factor of two in the space density measurement (Pretorius & Knigge 2012).

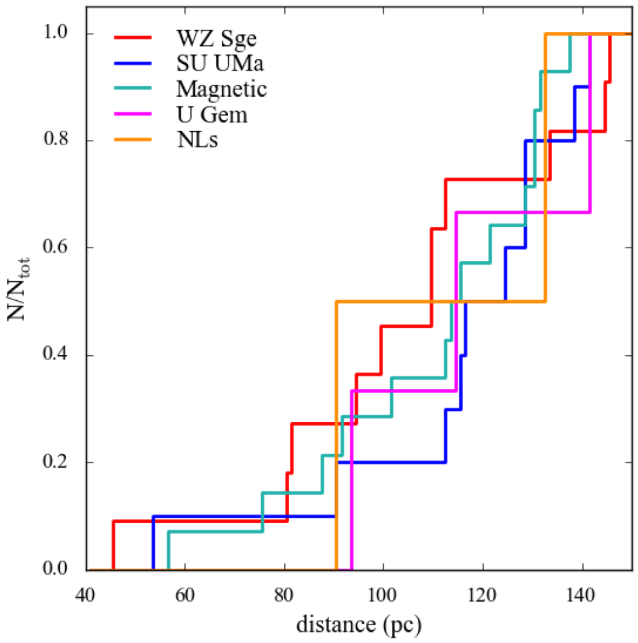

Figure 13. Cumulative distribution of the 150 pc CVs as a function of the distance for the different subtypes. The different distributions all show similar trends, suggesting the absence of clear selection effects in the 150 pc sample.

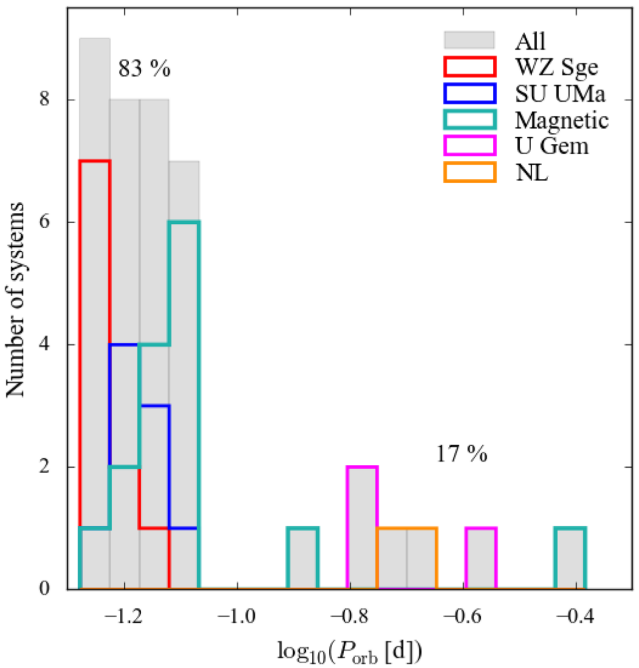

Figure 14. Period distribution for the CVs in the 150 pc sample. The majority of the systems are found below the period gap and, accounting also for the two WZ Sge-type stars without an orbital period determination, make up for ≃83 per cent of the observed systems.

Our measurement, $\rho_0 = (4.8^{+0.6}_{-0.8}) \times 10^{-6}$ pc^{-3}, is in good agreement with these previous estimates. However, using a volume-limited sample and the accurate astrometry of *Gaia*, we were able to reduce the uncertainty on the CV space density by an order of magnitude.

6 COMPARISON WITH THE MODELS OF CV EVOLUTION

6.1 The intrinsic population

The volume-limited sample of CVs obtained from *Gaia* provides, for the first time, a direct insight into the intrinsic properties of the Galactic population of CVs and allows a direct comparison between the observations and theoretical predictions.

Most models of CV evolution predict that ≃99 per cent of the present-day CVs should be found below the period gap, with a large fraction of them (≃40–70 per cent) having already evolved through the period minimum (Kolb 1993; Howell et al. 2001; Goliasch & Nelson 2015). The results from *Gaia* show instead a different picture, with (83 ± 6) per cent of the CVs in the 150 pc sample below the period gap and (17 ± 6) per cent above (Fig. 14). More importantly, the *Gaia* 150 pc CV sample contains only three plausible candidate period bouncers, GD 552 (Unda-Sanzana et al. 2008), SDSS J102905.21+485515.2 (Thorstensen et al. 2016), and 1RXS J105010.3−140431 (Patterson 2011; Pala et al. 2017), with WZ Sge, V455 And, and EZ Lyn being three additional weaker candidates (they all have brown-dwarf companions, but are right at the period minimum). Thus, seven to at most 14 per cent of the 150 pc CVs below the gap are period bouncers, a much smaller fraction than predicted by the population models. This discrepancy could reflect the selection biases discussed earlier; i.e. it could be possible that a number of period bouncers have not yet been identified because of their low quiescent variability and long outburst recurrence time. Assuming that the *Gaia* 150 pc CV sample is 77 per cent complete (Section 4), ≃12 CVs are still to be identified within 150 pc. The most favourable case in which all these are period bouncers would result in a fraction of (31 ± 7) per cent, bringing the observations into a marginal agreement with the prediction by Goliasch & Nelson (2015), ≃40 per cent, although the fraction of CVs above, (13 ± 5) per cent, and below the gap, (87 ± 5) per cent, would still be quite different from the theoretical predictions.

This observed disagreement can be potentially resolved by accounting for the presence of additional AML mechanisms besides the mere MB and GWR. Schreiber et al. (2016) proposed a model in which an empirical consequential AML (eCAML), i.e. a mechanism of AML arising from the mass transfer process itself, is generated by the friction between the secondary star and the white dwarf ejecta during nova explosions. The eCAML could lead to dynamically unstable mass transfer in CVs hosting low-mass white dwarfs, which would not survive as semidetached binaries but would merge into single objects (see also Nelemans et al. 2016). As a consequence, the fraction of CVs above and below the period gap would become, respectively, ≃85 and ≃15 per cent, and would be in good agreement with that derived from the analysis of the *Gaia* 150 pc CV sample, (83 ± 6) and (17 ± 6) per cent, even when accounting for incompleteness, (87 ± 5) and (13 ± 5) per cent. The space density predicted by the eCAML model, $\rho_0 \lesssim 2 \times 10^{-5}$ pc^{-3} (Belloni et al. 2018), is about a factor of 4 higher than the space density derived from the study of the *Gaia* 150 pc sample, $\rho_0 = (4.8^{+0.6}_{-0.8}) \times 10^{-6}$ pc^{-3}. This difference likely reflects the general uncertainties on the parameters (such as initial mass ratio distribution, initial separation distribution, initial binary fraction, common-envelope and magnetic braking efficiency) employed in binary population synthesis studies. Moreover, the space density derived by Belloni et al. (2018) has been derived from a CV population consisting of 80 per cent period bouncers, while the

fraction of such systems is only seven per cent in the observed 150 pc sample. Considering only systems that have not evolved through the period minimum yet, the space density predicted by the eCAML model, $\rho_0 \approx 4.5^{+4.5}_{-2.3} \times 10^{-6}\,\mathrm{pc}^{-3}$ (Belloni et al. 2020), perfectly agrees with the observation. This implies that either the large fraction of period bounce CVs still has to be identified (although this is not likely the case; see Section 4.2.2) or the current models fail to properly describe the post-period minimum evolution of CVs. Alternatively, it is possible that the time-scales required for a CV to evolve to the period minimum are much longer than current models (including eCAML) suggest.

Finally, we note in passing that the 150 pc sample contains some of the most peculiar CVs known:

(i) AR UMa is the polar with the highest magnetic field, $\langle B \rangle = 230$ MG (Schmidt et al. 1996). This suggests that strong magnetic fields are probably not as rare as thought (Ferrario, de Martino & Gänsicke 2015) and underlines the urgency to better understand the origin of magnetic CVs.

(ii) AE Aqr is a post-thermal time-scale mass transfer system (see Section 6.4). It is also an IP, with the fastest spinning white dwarf, $P_{\mathrm{spin}} = 33$ s (Patterson et al. 1980), among all CVs. This rapid spin results in a propeller mechanism that prevents the mass lost from the donor to reach the white dwarf surface, and is instead expelled in the surrounding space.

(iii) EZ Lyn is characterized by quasi-periodic brightening events superimposed on to sinusoidal photometric modulations (Zharikov et al. 2008, 2013) that, in the case of its twin system SDSS J123813.73−033933.0, have been interpreted as the interplay between spiral arms and small amplitude thermal instabilities in the accretion disc (Pala et al. 2019). Similar behaviour, although less periodic, has been observed also in GW Lib, where it could be associated with fluctuation in the mass accretion rate (Toloza et al. 2016).

(iv) V445 And, 'the CV that has it all', displays a grazing eclipse, permanent superhumps, non-radial white dwarf pulsations, and a spectroscopic period much longer ($P_{\mathrm{spec}} \simeq 3.5$ h) than the orbital one ($P_{\mathrm{orb}} \simeq 81.08$ min; Araujo-Betancor et al. 2005a), the origin of which is still not understood.

The prevalence of several of such peculiar systems suggests that the Galactic population of CVs is intrinsically very variegated and that these systems do not represent exceptional cases. The unexpected behaviour of systems like EZ Lyn and V455 And suggests that the physics describing the accretion process is still far from being completely understood. Moreover, the existence of systems such as AR UMa and AE Aqr is not accounted for by the model of CV evolution and provides another clue of the incompleteness of the current theories describing the evolution of close interacting binaries.

6.2 Mass accretion rates and white dwarf masses

Mass accretion results in compressional heating of the white dwarfs in CVs (Sion 1995; Townsley & Bildsten 2004), and therefore, the white dwarf effective temperature (T_{eff}) provides a direct measurement of its secular mean accretion rate ($\langle \dot{M} \rangle$; Townsley & Bildsten 2003). The different efficiencies of MB and GWR in removing angular momentum from the binary orbit (Section 1) cause long-period CVs to have $\langle \dot{M} \rangle$ about one order of magnitude higher compared to those of short-period CVs. Consequently, long-period systems should host hotter white dwarfs compared to short-period systems and hence T_{eff} measurements provide a direct insight into the evolutionary stage of the systems (Townsley & Gänsicke 2009; Pala et al. 2017).

Among the 42 CVs found within 150 pc, 21 have a published T_{eff} that can be considered reliable[8] and we can hence estimate their $\langle \dot{M} \rangle$ using equation (2) from Townsley & Gänsicke (2009). Table 5 lists the corresponding T_{eff} values as compiled from Townsley & Gänsicke (2009) and Pala et al. (2017), and includes four additional systems EZ Lyn, GD 552, Z Cha, and V355 UMa. For the systems for which the T_{eff} from the literature has been determined via spectroscopic analyses assuming $\log g = 8$, we recomputed the corresponding T_{eff} for $\log g = 8.35$ using equation (1) from Pala et al. (2017), in order to reflect the average observed mass of CV white dwarfs: $M_{\mathrm{WD}} \simeq 0.8\,\mathrm{M}_{\odot}$, i.e. $\log g = 8.35$. The errors on $\langle \dot{M} \rangle$ have been derived accounting for the uncertainties on both T_{eff} and the white dwarf mass (M_{WD}). For EZ Lyn, VY Aqr, and V355 UMa, we adopt ten per cent of their T_{eff} values as uncertainty, as no errors on T_{eff} were published. For the systems without a mass measurement, we assumed $M_{\mathrm{WD}} = 0.83 \pm 0.23\,\mathrm{M}_{\odot}$, corresponding to the average mass of CV white dwarfs (Zorotovic, Schreiber & Gänsicke 2011).

The left-hand panel of Fig. 15 shows the effective temperature as a function of the orbital period. For comparison, also the values from Townsley & Gänsicke (2009) and Pala et al. (2017) are reported, together with the evolutionary tracks for a typical CV ($M_{\mathrm{WD}} = 0.8\,\mathrm{M}_{\odot}$, with an initial secondary mass of $M_2 = 0.65\,\mathrm{M}_{\odot}$ and an initial $P_{\mathrm{orb}} = 12$ h; Pala et al. 2017). With only two 150 pc CVs having a T_{eff} at $P_{\mathrm{orb}} \gtrsim 180$ min, the comparison with these tracks is only meaningful at short orbital periods. The T_{eff} distribution of the intrinsic population shows some fundamental discrepancies between the theory and the observations that have been already highlighted by Pala et al. (2017) from the study of a large sample of CVs observed with the *Hubble Space Telescope*. In particular, the systems at the period minimum are characterized by a large scatter in T_{eff} as the white dwarf temperatures due to compressional heating are very sensitive to the white dwarf mass (Townsley & Gänsicke 2009). The recent work by Belloni et al. (2020) has shown that the mass distribution of CV white dwarfs is indeed the main reason behind this spread. Moreover, the systems below the period gap host hotter white dwarfs than suggested by the standard models (black track). This is also true in the case of the period bouncer track, which appears to be steeper than the theoretical predictions. As already discussed by Pala et al. (2017), these findings suggest that additional AML mechanisms are present (red track) besides pure GR in this period range. These additional AML mechanisms could also imply that period bounce CVs evolve faster than predicted by the models potentially explaining the lack of such evolved systems in the intrinsic population.

As shown in Fig. 15 (left), the effective temperatures of systems with similar orbital periods but different distances (coloured against grey points) are fully consistent with each other, allowing us to rule out the presence of observational biases as possible explanation for the discrepancies between theory and observations. Our results,

[8]Following the prescription by Townsley & Gänsicke (2009), a T_{eff} measurement is considered reliable when it has been derived (i) from the analysis of an ultraviolet spectrum in which the white dwarf signature has been unambiguously identified from the detection of a broad Ly α absorption profile and, possibly, sharp absorption metal lines, or (ii) from the analysis of the eclipse light curve in which both the white dwarf ingress and egress have been clearly detected.

Table 5. Literature effective temperatures and masses for the CV white dwarfs in the 150 pc sample, ordered according to their orbital periods.

System	$P_{\rm orb}$ (min)	$T_{\rm eff}$ (K)	$\langle\dot{M}\rangle$ ($\times10^{-11}$ M$_\odot$ yr^{-1})	$M_{\rm WD}$ (M$_\odot$)	Comment	References
GW Lib	76.78	16 995 ± 812 ↓	13 ± 3	0.84 ± 0.02	Pulsating, brightenings	17, 21
BW Scl	78.23	15 480 ± 900	10 ± 7	–		16
V627 Peg	78.51	16 292 ± 753	13 ± 9	–		17
V455 And	81.08	11 799 ± 750	4 ± 2	–	Eclipsing, pulsating	8
WZ Sge	81.63	14 900 ± 250	7.4 ± 1.3	0.85 ± 0.04		1, 2
V355 UMa	82.52	12 924 ± 1250	5 ± 4	–	Pulsating	33
EZ Lyn	84.97	13 595 ± 99	6 ± 4	–	Pulsating, brightenings	27
1RXS J105010.3−140431	88.56	11 622 ± 277	3 ± 2	–	Period bouncer candidate	17
V2051 Oph	89.90	–	–	0.78 ± 0.06	Eclipsing	19, 28
VY Aqr	90.85	15 148 ± 100	10 ± 6	–		23
OY Car	90.89	15 000 ± 2000	8 ± 5	0.84 ± 0.04	Eclipsing	11, 12
EX Hya	98.26	–	–	0.790 ± 0.026	Magnetic	5, 6, 7, 32
VV Pup	100.44	12 251 ± 600	4 ± 3	–	Magnetic	20
V834 Cen	101.52	14 927 ± 900	10 ± 6	–	Magnetic	20
GD 552	102.73	11 118 ± 400	2.9 ± 1.9	–	Period bouncer candidate	9
HT Cas	106.05	14 000 ± 1000	22 ± 8	0.61 ± 0.04	Eclipsing	25, 26
VW Hyi	106.95	20 000 ± 1000	50 ± 34	$0.71^{+0.18}_{-0.26}$		3, 4
Z Cha	107.28	15 700 ± 550	10 ± 3	0.84 ± 0.09	Eclipsing	29, 30
MR Ser	113.47	14 816 ± 900	9 ± 6	–	Magnetic	20
BL Hyi	113.64	13 818 ± 900	7 ± 5	–	Magnetic	20
ST LMi	113.89	11 005 ± 500	2.8 ± 1.8	–	Magnetic	20
AM Her	185.65	19 800 ± 700	33 ± 17	$0.78^{+0.12}_{-0.17}$	Magnetic	10
IP Peg	227.82	–	–	1.16 ± 0.02	Eclipsing	24
U Gem	254.74	30 000 ± 1000	31 ± 6	1.2 ± 0.05		14, 15
IX Vel	279.25	–	–	0.8 ± 0.2		31
SS Cyg	396.19	–	–	0.81 ± 0.19		22
AE Aqr	592.78	–	–	0.63 ± 0.05	Magnetic, evolved donor	13

Notes. For BW Scl, V455 And, V355 UMa, EZ Lyn, VY Aqr, VV Pup, V834 Cen, GD 552, MR Ser, BL Hyi, and ST LMi, the white dwarf $T_{\rm eff}$ reported in the literature has been determined via spectroscopic analyses assuming $\log g = 8$. However, this assumption does not reflect the average mass of CV white dwarfs: $M_{\rm WD} \simeq 0.8\,{\rm M}_\odot$, i.e. $\log g = 8.35$. For these systems, the $T_{\rm eff}$ values reported in this table have been recomputed for $\log g = 8.35$ using equation (1) from Pala et al. (2017).

References: (1) Sion et al. (1995), (2) Steeghs et al. (2007), (3) Gänsicke & Beuermann (1996), (4) Smith, Haswell & Hynes (2006), (5) Eisenbart et al. (2002), (6) Belle et al. (2003), (7) Beuermann & Reinsch (2008), (8) Araujo-Betancor et al. (2005a), (9) Unda-Sanzana et al. (2008), (10) Gänsicke et al. (2006), (11) Horne et al. (1994), (12) Littlefair et al. (2008), (13) Echevarría et al. (2008), (14) Long, Brammer & Froning (2006), (15) Echevarría, de la Fuente & Costero (2007), (16) Gänsicke et al. (2005), (17) Pala et al. (2017), (19) Baptista et al. (1998), (20) Araujo-Betancor et al. (2005a), (21) van Spaandonk et al. (2010), (22) Bitner, Robinson & Behr (2007), (23) Sion et al. (2003), (24) Copperwheat et al. (2010), (25) Feline et al. (2005), (26) Horne, Wood & Stiening (1991), (27) Szkody et al. (2013), (28) Saito & Baptista (2006), (29) Robinson et al. (1995), (30) Wade & Horne (1988), (31) Neustroev et al. (2011), (32) Suleimanov, Doroshenko & Werner (2019), and (33) Szkody et al. (2010).

instead, highlight the need for a revision of the current models of compact binary evolution.

Finally, the masses of 14 CV white dwarfs in the 150 pc sample are available in the literature (Table 5, right-hand panel of Fig. 15). The average mass is $\langle M_{\rm WD}\rangle = 0.83 \pm 0.17$, in perfect agreement with the measurement from Zorotovic et al. (2011), $\langle M_{\rm WD}\rangle = 0.83 \pm 0.23\,{\rm M}_\odot$. As also shown by Zorotovic et al. (2011), this result confirms that the higher mass of CV white dwarfs compared to that of single white dwarfs and their detached progenitors, $\langle M_{\rm WD}\rangle \simeq 0.6\,{\rm M}_\odot$ (Koester, Schulz & Weidemann 1979; Liebert, Bergeron & Holberg 2005b; Kepler et al. 2007), cannot be related to an observational bias.

The average mass of CV white dwarfs cannot be explained (i) invoking different parent populations for the present-day CVs and the present-day pre-CVs (e.g. Zorotovic et al. 2011) or (ii) assuming mass growth during nova cycles or through thermal time-scale mass transfer (Wijnen, Zorotovic & Schreiber 2015). Instead, the eCAML proposed by Schreiber et al. (2016) could mitigate the discrepancy between the theory and the observations. The eCAML leads to merger of the two stellar components in systems hosting low-mass white dwarfs, which would then disappear from the CV population, thus naturally explaining the observed high average mass of CV white dwarfs. Nonetheless, the exact mechanism behind the additional CAML and the reason for its dependence on white dwarf mass are unclear.

6.3 Magnetic systems

Pretorius, Knigge & Schwope (2013) derived the space density of magnetic CVs as $\rho_{\rm mCV} = 1.3^{+0.6}_{-0.4} \times 10^{-6}\,{\rm pc}^{-3}$. Comparing this value with the space density of non-magnetic CVs, $\rho_0 = 4^{+6}_{-2} \times 10^{-6}\,{\rm pc}^{-3}$, from Pretorius & Knigge (2012), implies that about one-third of CVs are magnetic.

From the analysis of the *Gaia* parallaxes, we found that a large fraction, (36 ± 7) per cent, of the CVs identified within 150 pc contain a magnetic white dwarf (Fig. 16). This corresponds to a space density[9] of $\rho_{\rm mCV} = 1.3^{+0.3}_{-0.4} \times 10^{-6}\,{\rm pc}^{-3}$ (Table 6), consistent with the result by Pretorius et al. (2013).

Magnetic CVs are thought to follow a different evolutionary path compared to the non-magnetic system. Owing to the coupling with

[9]Note that the values reported in Table 6 cannot be corrected for incompleteness since this would require the knowledge of the contribution of each subtype to the population of CVs that still has to be discovered.

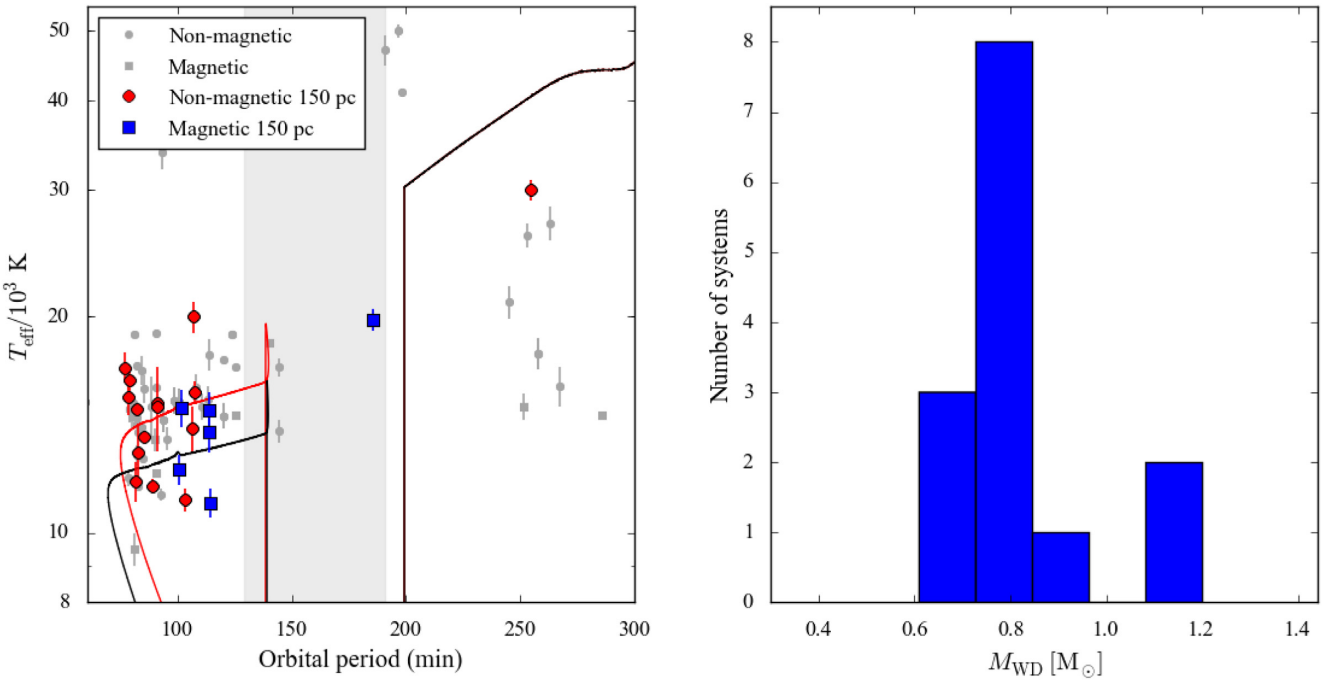

Figure 15. Left: Effective temperature for magnetic (squares) and non-magnetic (circles) CV white dwarfs from Townsley & Gänsicke (2009) and Pala et al. (2017) (grey). Magnetic and non-magnetic systems within 150 pc from Table 5 are shown in blue and red, respectively. The period gap is highlighted by the grey band. The solid lines represent the evolutionary tracks from Pala et al. (2017) for a typical CV ($M_{\rm WD} = 0.8\,{\rm M}_\odot$, with an initial secondary mass of $M_2 = 0.65\,{\rm M}_\odot$ and an initial $P_{\rm orb} = 12$ h) in which AML is driven by both MB and GWR above the period gap, while below the period gap only GWR (black) or GWR plus a residual MB (red) drive the evolution of the system. Right: White dwarf mass distribution for the CVs in the 150 pc sample as reported from the literature (Table 5).

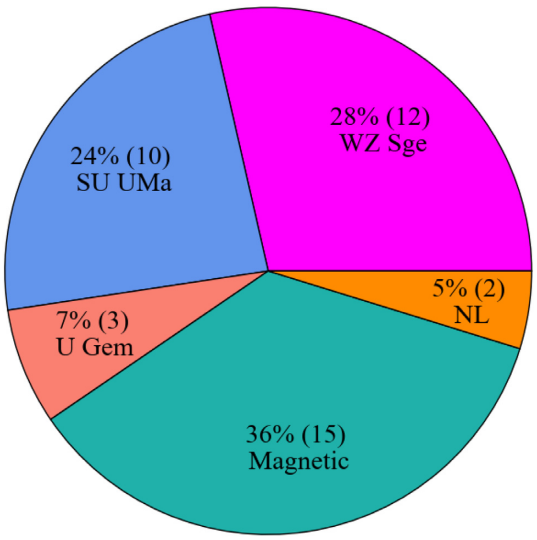

Figure 16. CV subtype contribution to the 150 pc sample. More than one-third of the observed CVs host a magnetic white dwarf, in clear contrast with the total absence of magnetic white dwarfs in the parent population of PCEBs (Liebert et al. 2005a, 2015).

the magnetic field of the white dwarf, MB is reduced or even completely suppressed in the system with the strongest magnetic fields (Li, Wu & Wickramasinghe 1994). Consequently, IPs and polars evolve slower than non-magnetic CVs, thus explaining the high fraction of observed magnetic CVs (Araujo-Betancor et al. 2005b).

However, this high incidence of magnetism in CVs is not reflected in the fraction of magnetic white dwarfs observed in their parent population, i.e. the PCEBs, with no confirmed magnetic white dwarf detected in any of these detached binaries (Liebert et al. 2005a, 2015). Different scenarios have been proposed to explain the observed fraction of magnetic CVs, such as Ap and Bp progenitors that preserve a fossil magnetic field while becoming white dwarfs (Angel, Borra & Landstreet 1981), or interaction during the common-envelope phase (Tout et al. 2008). However, they have been unable to explain the lack of magnetic white dwarfs in the population of PCEB, and consequently, the origin of magnetic CVs remains unclear.

Table 6. Space densities for different CV subtypes computed considering the volume enclosed within $d_{\rm lim} = 150$ pc assuming a scale height $h = 280$ pc.

Subtype	$N_{\rm CV}$	$N_{\rm CV}/N_{\rm tot}$ (per cent)	ρ_0 ($\times 10^{-6}$ pc^{-3})
WZ Sge	12	28 ± 7	1.0 ± 0.3
SU UMa	10	24 ± 7	$0.8^{+0.2}_{-0.4}$
U Gem	3	7 ± 4	$0.2^{+0.2}_{-0.1}$
NL	2	5 ± 3	$0.15^{+0.2}_{-0.3}$
Magnetic	15	36 ± 7	$1.3^{+0.3}_{-0.4}$

6.4 Systems with an evolved donor

The stability of the mass transfer process requires a mass ratio $q = M_2/M_{\rm WD} \lesssim 1$ (where M_2 is the mass of the secondary star; Frank, King & Raine 2002). However, it has been shown that CVs hosting massive donors ($M_2 \simeq 1.5\,{\rm M}_\odot$) could survive a phase of thermal time-scale mass transfer during which the accreted material

burns steadily on to the white dwarf (Schenker et al. 2002). During the thermal time-scale mass transfer, the donor is stripped of its envelope and the surviving system is a normal CV in which the white dwarf accretes from the remnant core of its companion, rich in CNO processed material. These CVs are predicted to make up for ≃30 per cent of the Galactic CV population (Schenker et al. 2002).

These systems can be easily recognized in the ultraviolet from their enhanced N V/C IV line flux ratios compared to those of CVs that have formed through the standard channel and the observed fraction of CVs with an evolved donor has been found to be ≃15 per cent (Gänsicke et al. 2003). In the 150 pc CV sample, we identified only two of such CVs: AE Aqr (Jameson, King & Sherrington 1980) and V2301 Oph (Schmidt & Stockman 2001), corresponding to a fraction of (5 ± 3) per cent. The higher fraction found by Gänsicke et al. (2003) can be explained by an observational bias; these systems host more massive (and hence larger) and brighter donors compared to those of normal CVs and therefore are easily detected even at large distances. Instead, the theoretically predicted fraction by Schenker et al. (2002), 30 per cent, is much higher compared to the observed fraction of CV with evolved donors in the 150 pc sample.

CVs with evolved donors represent an evolutionary link between CVs and the more compact AM CVn stars. The formation of the latter is still poorly understood, but three different pathways have been proposed (Nelemans 2005). In the first scenario, the systems are formed from a double white dwarf binary in which the less massive star is brought to contact with its Roche lobe by the orbital shrinkage due to GWR. Alternatively, the progenitors could be a binary containing a white dwarf plus a non-degenerate, helium core burning star. Finally, AM CVn could descend from CVs with an evolved donor. Hosting massive secondary stars, these systems are able to evolve to $P_{\rm orb}$ much shorter than the period minimum. Owing to the mass transfer process, the secondary is progressively eroded, till only its helium-rich core is left and an AM CVn star is born. The fraction of CVs with an evolved donor that we derived could provide an upper limit on the number of AM CVn that are expected to form through this channel, yielding a valuable observational test for the contribution of the different formation channels to the overall population of these compact systems.

7 TERTIARY COMPANIONS

The formation and the evolution of a binary can be influenced by the presence of a nearby third body orbiting the system. For example, the third body can give rise to Lidov–Kozai cycles that can induce periodical variation in the eccentricity and the inclination of the inner binary with respect to the orbital plane of the external body (see Naoz 2016, for a review). This gravitational interaction can hence affect the mass transfer process and potentially even lead to mergers (e.g. Toonen, Hamers & Portegies Zwart 2016). In order to fully constrain the formation and evolution of CVs, it is important to assess the multiplicity fractions of these systems.

In the past, the most successful method to identify wide-orbit companions was the identification of period modulations in the long-term light curves of the system and several studies have suggested that some CVs could be part of triple systems. Few examples are VY Scl (Martínez-Pais et al. 2000), DP Leo (Beuermann et al. 2011), FS Aur (Chavez et al. 2012), and LX Ser (Li et al. 2017), which have been suggested to host circumbinary substellar objects or giant planets. However, the observed modulations could also be explained by the magnetic activity of the donor star, and owing to the lack of a direct detection of the third bodies, it is difficult to disentangle the two scenarios.

The accurate parallaxes and proper motions delivered by the *Gaia* space mission in its DR2 offer the first opportunity to carry out a systematic search for third components on wide orbits to the 150 pc CVs by searching for common proper motion companions.

In order to identify these objects, we performed a cone search of 3 pc radius around each of the 150 pc CVs, and selected those objects for which

$$\Delta = \sqrt{\left(\frac{\Delta\mu_{\rm RA}}{\sigma_{\mu_{\rm RA}}}\right)^2 + \left(\frac{\Delta\mu_{\rm Dec}}{\sigma_{\mu_{\rm Dec}}}\right)^2} < 3, \quad (7)$$

where $\Delta\mu$ are the differences in the proper motion components and σ_μ are the quadrature sums of the corresponding 3σ uncertainties.

We find that two CVs, V379 Tel and *Gaia* J154008.28−392917.6, satisfy this condition. Using the *Gaia* coordinates and parallaxes, we computed the separation between the inner binary and the third body that gave $D \simeq 2.5$ pc (Table 7). Although it did not satisfy the previous condition ($\Delta \simeq 11$), we cannot ignore that *Gaia* J051903.99+630340.4 has a nearby companion (TYC 4084-172-1) located at a similar distance (≃2.2 pc), and therefore, we also include this object in the following discussion.

Given the relatively large orbital separations, we computed the gravitational binding energy

$$-E_{\rm bind} = G\frac{(M_{\rm WD} + M_2)M_3}{D} \quad (8)$$

of each triplet assuming that the inner binary is a typical short-period CV (as the three systems listed in Table 7 are all located below the period gap), with a white dwarf of mass $M_{\rm WD} = 0.83\,{\rm M}_\odot$ and a donor of mass $M_2 = 0.14\,{\rm M}_\odot$, typical of a CV below the period gap (Knigge et al. 2011). We assumed that the third body is on a circular orbit around the inner binary and we estimated their possible masses accordingly to their position on the Hertzsprung–Russell diagram (Fig. 17). The third companions result being an M-dwarf of spectral type ≃M2V (as we estimated using as a reference the table[10] from Pecaut & Mamajek 2013), a white dwarf, and a G-type star for V379 Tel, *Gaia* J154008.28−392917.6, and *Gaia* J051903.99+630340.4, respectively. We therefore assumed

(i) $M_3 = 0.4\,{\rm M}_\odot$, corresponding to the mass of an M2V star (Pecaut & Mamajek 2013), in the case of the tertiary companion of V379 Tel;

(ii) $M_3 = 0.6\,{\rm M}_\odot$, corresponding to the average mass of single white dwarfs (Liebert et al. 2005b), in the case of the tertiary companion of *Gaia* J154008.28−392917.6;

(iii) $M_3 = 1\,{\rm M}_\odot$ in the case of TYC 4084-172-1, given its spectral type G3V and surface gravity of $\log(g) = 4.2(2)$ (Frasca et al. 2018; see also Fig. C2).

The binding energies we derived are listed in Table 7. The related uncertainties have been computed accounting for those on the *Gaia* coordinates and parallaxes of each pair of objects, and are dominated by the latter. At this stage, their large values combined with the unknown uncertainties related to the theoretical limit for stellar binding energies, $-E_{\rm bind} \approx 1 \times 10^{41}$ (Burgasser et al. 2007), make it impossible to unambiguously establish whether these CVs are

[10] http://www.pas.rochester.edu/~emamajek/EEM_dwarf_UBVIJHK_colors_Teff.txt

Table 7. 150 pc CVs with a common proper motion companion.

System	*Gaia* DR2 ID	$P_{\rm orb}$ (min)	Type	ϖ (mas)	$\mu_{\rm RA}$ (mas yr^{-1})	$\mu_{\rm Dec}$ (mas yr^{-1})	Δ	Angular separation	(pc)	D (au)	$-E_{\rm bind}$ (erg)
V379 Tel	6658737220627065984	101.03	AM	7.65(7)	−60.8(1)	−17.75(9)	2.9	30.8″	2.3 ± 1.5	(5 ± 3) × 10^5	(1.5 ± 1.0) × 10^{40}
	6658737388128701184		M2V	7.52(5)	−60.64(8)	−18.44(6)					
Gaia J154008.28−392917.6	6008982469163902464	–	UGWZ	7.49(11)	64.8(2)	1.6(2)	2.4	1.1°	3 ± 13	(6 ± 26) × 10^5	(2 ± 8) × 10^{40}
	6002961479076981632		WD	7.6(8)	52(2)	4(1)					
Gaia J051903.99+630340.4	2859572775976582 40	126:	UGSU	8.59(4)	−13.07(5)	−45.30(5)	11	6.8″	2.2 ± 0.7	(4.6 ± 1.4) × 10^5	(3.7 ± 1.1) × 10^{40}
TYC 4084-172-1	2859572775976583 68		G3V	8.43(3)	−11.19(3)	−44.38(4)					

Notes. $-E_{\rm bind}$ has been computed assuming $M_3 = 0.4\,{\rm M}_\odot$, $M_3 = 0.6\,{\rm M}_\odot$, and $M_3 = 1\,{\rm M}_\odot$ for V379 Tel, *Gaia* J154008.28−392917.6, and *Gaia* J051903.99+630340.4, respectively.

Figure 17. Hertzsprung–Russell diagram of the *Gaia* sources within 150 pc (grey) showing, as a reference, the position occupied by the Sun (Casagrande & VandenBerg 2018) and by V379 Tel (pink), *Gaia* J154008.28−392917.6 (blue), and *Gaia* J051903.99+630340.4 (orange) and their common proper motion companions (black), which result being an M-dwarf, a white dwarf, and a G-type star, respectively.

part of hierarchical systems and additional observational efforts are required in order to finally assess their hierarchical structure.

8 CONCLUSIONS

Making use of the accurate astrometry delivered by the ESA *Gaia* space mission in its DR2, we carry out the first detailed study of the volume-limited sample of 42 CVs located within 150 pc. Combining the *Gaia* data with the photometric and spectroscopic observations from SDSS and CRTS, we estimate the sample to be (77 ± 10) per cent complete. This is mainly dictated by the efficiency of the discovery methods employed in detecting new CVs, which are biased towards systems accreting at intermediate mass rates, which can be easily detected in the X-rays or thanks to their dwarf nova outbursts.

Assuming $h = 280$ pc as a typical scale height for the Galactic CV population, we estimate the CV space density, which is $\rho_0 = (4.8^{+0.6}_{-0.8}) \times 10^{-6}$ pc^{-3}. Thanks to the exquisite *Gaia* data, we reduce the uncertainty on ρ_0 by a factor of 10 compared to the pre-*Gaia* estimates. The uncertainties we derive take well into account the estimated completeness of the sample and possible different values of the scale height in the range 100–500 pc. Nonetheless, given that the 150 pc CV sample is dominated by short-period systems representing the old component of the Galactic CV population, it is reasonable to assume that the larger values of h are likely the most realistic.

The advent of the *Gaia* space mission provides also the unique opportunity to study the intrinsic properties of the Galactic CV population and to constrain the models describing the formation and evolution of these systems. We find that the observed space density is significantly lower than that predicted by the current available models of CV evolution. Moreover, the fractions of CVs above (17 per cent) and below (83 per cent) the period gap are in clear disagreement with the theoretical predictions (1 and 99 per cent, respectively). Both discrepancies can be resolved by the recently proposed eCAML model in which CVs hosting low-

mass white dwarfs merge owing to frictional AML arising from nova explosions. Consequently, the Galactic CV population would be composed of a lower absolute number of systems that would naturally imply a lower space density. Moreover, the fractions of CVs predicted by the eCAML model are 15 and 85 per cent above and below the period gap, respectively, in better agreement with the observed value. The disappearance of the CVs hosting low-mass white dwarfs would also be consistent with the average masses of the CV white dwarfs in the 150 pc sample, $\langle M_{\rm WD}\rangle = 0.83 \pm 0.17\,{\rm M}_{\odot}$, being higher than the masses of their detached progenitors (i.e. PCEB, $\langle M_{\rm WD}\rangle \simeq 0.6\,{\rm M}_{\odot}$; Zorotovic et al. 2011). The need to include additional mechanisms of AML in the models is also supported by the observed effective temperatures and, consequently, mass accretion rates of the 150 pc CVs, which, below the period gap, are found to be accreting at higher rates than theoretically predicted. However, the observed fraction of period bounce CVs, 7–14 per cent, is much lower than current models (including eCAML) predict, 40–80 per cent, and it is possible that the time-scales required for a CV to evolve to the period minimum are much longer than theoretically predicted.

Studying the composition of the 150 pc CV sample, we identify a large fraction of magnetic CVs, 36 per cent. This finding is particularly intriguing given that no confirmed magnetic white dwarf is known among the PCEBs. All the models proposed to explain the observed fraction of magnetic CVs predict also the existence of magnetic white dwarfs in PCEBs, and consequently, this high incidence of magnetism among CV white dwarfs remains unclear.

We also show that the fraction of CVs hosting nuclear evolved donors is $\simeq$5 per cent, lower than the pre-*Gaia* observational estimate, $\simeq$15 per cent. Most likely, this difference arises from an observational bias since these systems are brighter than normal CVs and are easily detected even at large distances. Moreover, the observed fraction of CVs with evolved donors is significantly lower than predicted by the theory (30 per cent).

Finally, we find that three CVs have a common proper motion companion. However, the lack of accurate system parameters does not allow to draw definite conclusion on whether they form hierarchical triple systems and additional observations are required to finally establish whether these common proper motion companion pairs are gravitationally bound.

ACKNOWLEDGEMENTS

This work has made use of data from the ESA mission *Gaia* (https://www.cosmos.esa.int/gaia), processed by the *Gaia* Data Processing and Analysis Consortium (DPAC, https://www.cosmos.esa.int/web/gaia/dpac/consortium). Funding for the DPAC has been provided by national institutions, in particular the institutions participating in the *Gaia* Multilateral Agreement.

The research leading to these results has received funding from the European Research Council under the European Union's Seventh Framework Programme (FP/2007–2013)/ERC Grant Agreement No. 320964 (WDTracer).

Based on observations made with ESO Telescopes at Paranal Observatory under programme ID 0101.C-0646(A).

Based on observations obtained under programme ID SO2018B-015 at the SOAR telescope, which is a joint project of the Ministério da Ciência, Tecnologia, Inovações e Comunicações (MCTIC) do Brasil, the U.S. National Optical Astronomy Observatory (NOAO), the University of North Carolina at Chapel Hill (UNC), and Michigan State University (MSU).

The research leading to these results has received funding from the European Research Council under the European Union's Horizon 2020 research and innovation programme no. 677706 (WD3D).

The work presented in this article made large use of TOPCAT and STILTS Table/VOTable Processing Software (Taylor 2005).

Funding for the SDSS and SDSS-II has been provided by the Alfred P. Sloan Foundation, the Participating Institutions, the National Science Foundation, the U.S. Department of Energy, the National Aeronautics and Space Administration, the Japanese Monbukagakusho, the Max Planck Society, and the Higher Education Funding Council for England. The SDSS website is http://www.sdss.org/.

The SDSS is managed by the Astrophysical Research Consortium for the Participating Institutions. The Participating Institutions are the American Museum of Natural History, Astrophysical Institute Potsdam, University of Basel, University of Cambridge, Case Western Reserve University, University of Chicago, Drexel University, Fermilab, the Institute for Advanced Study, the Japan Participation Group, Johns Hopkins University, the Joint Institute for Nuclear Astrophysics, the Kavli Institute for Particle Astrophysics and Cosmology, the Korean Scientist Group, the Chinese Academy of Sciences (LAMOST), Los Alamos National Laboratory, the Max Planck Institute for Astronomy (MPIA), the Max Planck Institute for Astrophysics (MPA), New Mexico State University, Ohio State University, University of Pittsburgh, University of Portsmouth, Princeton University, the United States Naval Observatory, and the University of Washington.

Funding for SDSS-III has been provided by the Alfred P. Sloan Foundation, the Participating Institutions, the National Science Foundation, and the U.S. Department of Energy Office of Science. The SDSS-III website is http://www.sdss3.org/.

SDSS-III is managed by the Astrophysical Research Consortium for the Participating Institutions of the SDSS-III Collaboration including the University of Arizona, the Brazilian Participation Group, Brookhaven National Laboratory, Carnegie Mellon University, University of Florida, the French Participation Group, the German Participation Group, Harvard University, the Instituto de Astrofisica de Canarias, the Michigan State/Notre Dame/JINA Participation Group, Johns Hopkins University, Lawrence Berkeley National Laboratory, Max Planck Institute for Astrophysics, Max Planck Institute for Extraterrestrial Physics, New Mexico State University, New York University, Ohio State University, Pennsylvania State University, University of Portsmouth, Princeton University, the Spanish Participation Group, University of Tokyo, University of Utah, Vanderbilt University, University of Virginia, University of Washington, and Yale University.

AA acknowledges generous supports from Naresuan University. MRS thanks for support from the Fondo Nacional de Desarrollo Científico y Tecnológico (FONDECYT, grant 1181404). OT was supported by a Leverhulme Trust Research Project Grant. BTG and OT were supported by the UK Science and Technology Facilities Council (STFC) grant ST/P000495.

REFERENCES

Ak T., Bilir S., Ak S., Retter A., 2007, New Astron., 12, 446
Angel J. R. P., Borra E. F., Landstreet J. D., 1981, ApJS, 45, 457
Araujo-Betancor S. et al., 2005a, A&A, 430, 629
Araujo-Betancor S., Gänsicke B. T., Long K. S., Beuermann K., de Martino D., Sion E. M., Szkody P., 2005b, ApJ, 622, 589
Bailer-Jones C. A. L., 2015, PASP, 127, 994
Bailey J., 1981, MNRAS, 197, 31

Banzatti A., Pascucci I., Edwards S., Fang M., Gorti U., Flock M., 2019, ApJ, 870, 76
Baptista R., Catalan M. S., Horne K., Zilli D., 1998, MNRAS, 300, 233
Belle K. E., Howell S. B., Sion E. M., Long K. S., Szkody P., 2003, ApJ, 587, 373
Belloni D., Schreiber M. R., Zorotovic M., Iłkiewicz K., Hurley J. R., Giersz M., Lagos F., 2018, MNRAS, 478, 5626
Belloni D., Schreiber M. R., Pala A. F., Gänsicke B. T., Zorotovic M., Rodrigues C. V., 2020, MNRAS, 491, 5717
Belloni T., Verbunt F., Schmitt J. H. M. M., 1993, A&A, 269, 175
Bernardini F., de Martino D., Falanga M., Mukai K., Matt G., Bonnet-Bidaud J.-M., Masetti N., Mouchet M., 2012, A&A, 542, A22
Beuermann K., 2006, A&A, 460, 783
Beuermann K., Reinsch K., 2008, A&A, 480, 199
Beuermann K., Schwope A., Weissieker H., Motch C., 1985, Space Sci. Rev., 40, 135
Beuermann K., Harrison T. E., McArthur B. E., Benedict G. F., Gänsicke B. T., 2003, A&A, 412, 821
Beuermann K. et al., 2011, A&A, 526, A53
Bitner M. A., Robinson E. L., Behr B. B., 2007, ApJ, 662, 564
Breedt E. et al., 2014, MNRAS, 443, 3174
Burgasser A. J., Reid I. N., Siegler N., Close L., Allen P., Lowrance P., Gizis J., 2007, in Reipurth B., Jewitt D., Keil K., eds, Protostars and Planets V. University of Arizona Press, Tucson, AZ, p. 427
Casagrande L., VandenBerg D. A., 2018, MNRAS, 479, L102
Chavez C. E., Tovmassian G., Aguilar L. A., Zharikov S., Henden A. A., 2012, A&A, 538, A122
Clemens J. C., Crain J. A., Anderson R., 2004, in Moorwood A. F. M., Iye M., eds, Proc. SPIE Conf. Ser. Vol. 5492, Ground-Based Instrumentation for Astronomy. SPIE, Bellingham, p. 331
Copperwheat C. M., Marsh T. R., Dhillon V. S., Littlefair S. P., Hickman R., Gänsicke B. T., Southworth J., 2010, MNRAS, 402, 1824
Dawson K. S. et al., 2013, AJ, 145, 10
de Kool M., 1992, A&A, 261, 188
Denisenko D., 2018, Astron. Telegram, 11917, 1
Denisenko D. V., Larin I., 2018, preprint (arXiv:1807.04574)
Downes R. A., Webbink R. F., Shara M. M., Ritter H., Kolb U., Duerbeck H. W., 2001, PASP, 113, 764
Drake A. J. et al., 2009, ApJ, 696, 870
Drake A. J. et al., 2014, MNRAS, 441, 1186
Duerbeck H. W., 1999, Inf. Bull. Var. Stars, 4731, 1
Echevarría J., de la Fuente E., Costero R., 2007, AJ, 134, 262
Echevarría J., Smith R. C., Costero R., Zharikov S., Michel R., 2008, MNRAS, 387, 1563
Eisenbart S., Beuermann K., Reinsch K., Gänsicke B. T., 2002, A&A, 382, 984
Fang M. et al., 2018, ApJ, 868, 28
Feline W. J., Dhillon V. S., Marsh T. R., Watson C. A., Littlefair S. P., 2005, MNRAS, 364, 1158
Ferrario L., de Martino D., Gänsicke B. T., 2015, Space Sci. Rev., 191, 111
Frank J., King A., Raine D. J., 2002, Accretion Power in Astrophysics. 3rd edn., Cambridge Univ. Press, Cambridge
Frasca A., Guillout P., Klutsch A., Ferrero R. F., Marilli E., Biazzo K., Gandolfi D., Montes D., 2018, A&A, 612, A96
Gaia Collaboration, 2016, A&A, 595, A1
Gaia Collaboration, 2018, A&A, 616, A1
Gänsicke B. T., 2005, in Hameury J.-M., Lasota J.-P., eds, ASP Conf. Ser. Vol. 330, The Astrophysics of Cataclysmic Variables and Related Objects. Astron. Soc. Pac., San Francisco, p. 3
Gänsicke B. T., Beuermann K., 1996, A&A, 309, L47
Gänsicke B. T., Koester D., 1999, A&A, 346, 151
Gänsicke B. T., Sion E. M., Beuermann K., Fabian D., Cheng F. H., Krautter J., 1999, A&A, 347, 178
Gänsicke B. T. et al., 2003, ApJ, 594, 443
Gänsicke B. T., Szkody P., Howell S. B., Sion E. M., 2005, ApJ, 629, 451
Gänsicke B. T., Long K. S., Barstow M. A., Hubeny I., 2006, ApJ, 639, 1039
Gänsicke B. T. et al., 2009, MNRAS, 397, 2170
Gentile Fusillo N. P. et al., 2019, MNRAS, 482, 4570
Goliasch J., Nelson L., 2015, ApJ, 809, 80
Graham M. J. et al., 2019, PASP, 131, 078001
Hamann F., Persson S. E., 1992, ApJS, 82, 247
Hameury J.-M., Menou K., Dubus G., Lasota J.-P., Hure J.-M., 1998, MNRAS, 298, 1048
Harrison T. E., Johnson J. J., McArthur B. E., Benedict G. F., Szkody P., Howell S. B., Gelino D. M., 2004, AJ, 127, 460
Hernández Santisteban J. V., Knigge C., Pretorius M. L., Sullivan M., Warner B., 2018, MNRAS, 473, 3241
Hodgkin S. T., Wyrzykowski L., Blagorodnova N., Koposov S., 2013, Phil. Trans. R. Soc. A, 371, 20120239
Hollands M. A., Tremblay P.-E., Gänsicke B. T., Gentile-Fusillo N. P., Toonen S., 2018, MNRAS, 480, 3942
Horne K., Wood J. H., Stiening R. F., 1991, ApJ, 378, 271
Horne K., Marsh T. R., Cheng F. H., Hubeny I., Lanz T., 1994, ApJ, 426, 294
Howell S. B., Nelson L. A., Rappaport S., 2001, ApJ, 550, 897
Jameson R. F., King A. R., Sherrington M. R., 1980, MNRAS, 191, 559
Kato T. et al., 2015, PASJ, 67, 105
Kato T. et al., 2016, PASJ, 68, 65
Kepler S. O., Kleinman S. J., Nitta A., Koester D., Castanheira B. G., Giovannini O., Costa A. F. M., Althaus L., 2007, MNRAS, 375, 1315
Knigge C., Baraffe I., Patterson J., 2011, ApJS, 194, 28
Kochanek C. S. et al., 2017, PASP, 129, 104502
Koester D., Schulz H., Weidemann V., 1979, A&A, 76, 262
Kolb U., 1993, A&A, 271, 149
Kulkarni S. R., 2013, Astron. Telegram, 4807, 1
Larin I., Denisenko D., Pogrebisskiy S., 2018, Astron. Telegram, 11401, 1
Law N. M. et al., 2009, PASP, 121, 1395
Lépine S., Bergeron P., Lanning H. H., 2011, AJ, 141, 96
Li J. K., Wu K. W., Wickramasinghe D. T., 1994, MNRAS, 268, 61
Li K. et al., 2017, PASJ, 69, 28
Liebert J. et al., 2005a, AJ, 129, 2376
Liebert J., Bergeron P., Holberg J. B., 2005b, ApJS, 156, 47
Liebert J., Ferrario L., Wickramasinghe D. T., Smith P. S., 2015, ApJ, 804, 93
Lindegren L., Lammers U., Hobbs D., O'Mullane W., Bastian U., Hernández J., 2012, A&A, 538, A78
Lindegren L. et al., 2018, A&A, 616, A2
Linnell A. P., Godon P., Hubeny I., Sion E. M., Szkody P., 2007, ApJ, 662, 1204
Linnell A. P., Godon P., Hubeny I., Sion E. M., Szkody P., Barrett P. E., 2009, ApJ, 703, 1839
Lipunov V. et al., 2010, Adv. Astron., 2010, 349171
Littlefair S. P., Dhillon V. S., Marsh T. R., Gänsicke B. T., Southworth J., Watson C. A., 2006, Science, 314, 1578
Littlefair S. P., Dhillon V. S., Marsh T. R., Gänsicke B. T., Southworth J., Baraffe I., Watson C. A., Copperwheat C., 2008, MNRAS, 388, 1582
Liu W.-M., Li X.-D., 2019, ApJ, 870, 22
Long K. S., Brammer G., Froning C. S., 2006, ApJ, 648, 541
Luri X. et al., 2018, A&A, 616, A9
McAllister M. J. et al., 2017, MNRAS, 467, 1024
McAllister M. J. et al., 2019, MNRAS, 486, 5535
McArthur B. E. et al., 2001, ApJ, 560, 907
Martínez-Pais I. G., Martín-Hernández N. L., Casares J., Rodríguez-Gil P., 2000, ApJ, 538, 315
Maza J., Gonzalez L. E., 1983, Int. Astron. Union Circ., 3854, 2
Meyer F., Meyer-Hofmeister E., 1984, A&A, 132, 143
Miller-Jones J. C. A., Sivakoff G. R., Knigge C., Körding E. G., Templeton M., Waagen E. O., 2013, Science, 340, 950
Naoz S., 2016, ARA&A, 54, 441
Natta A., Testi L., Alcalá J. M., Rigliaco E., Covino E., Stelzer B., D'Elia V., 2014, A&A, 569, A5
Nelemans G., 2005, in Hameury J.-M., Lasota J.-P., eds, ASP Conf. Ser. Vol. 330, The Astrophysics of Cataclysmic Variables and Related Objects. Astron. Soc. Pac., San Francisco, p. 27

Nelemans G., Siess L., Repetto S., Toonen S., Phinney E. S., 2016, ApJ, 817, 69
Neustroev V. V., Suleimanov V. F., Borisov N. V., Belyakov K. V., Shearer A., 2011, MNRAS, 410, 963
Neustroev V. V. et al., 2017, MNRAS, 467, 597
Nisini B., Antoniucci S., Alcalá J. M., Giannini T., Manara C. F., Natta A., Fedele D., Biazzo K., 2018, A&A, 609, A87
Osaki Y., 1974, PASJ, 26, 429
Paczynski B., Sienkiewicz R., 1983, ApJ, 268, 825
Pala A. F. et al., 2017, MNRAS, 466, 2855
Pala A. F., Schmidtobreick L., Tappert C., Gänsicke B. T., Mehner A., 2018, MNRAS, 481, 2523
Pala A. F. et al., 2019, MNRAS, 483, 1080
Parsons S. G. et al., 2013, MNRAS, 429, 256
Patterson J., 1984, ApJS, 54, 443
Patterson J., 1998, PASP, 110, 1132
Patterson J., 2011, MNRAS, 411, 2695
Patterson J., Branch D., Chincarini G., Robinson E. L., 1980, ApJ, 240, L133
Patterson J., Thorstensen J. R., Kemp J., 2005, PASP, 117, 427
Pecaut M. J., Mamajek E. E., 2013, ApJS, 208, 9
Pogson N., 1857, MNRAS, 17, 200
Pojmanski G., 1997, Acta Astron., 47, 467
Politano M., 1996, ApJ, 465, 338
Pretorius M. L., Knigge C., 2012, MNRAS, 419, 1442
Pretorius M. L., Knigge C., Kolb U., 2007a, MNRAS, 374, 1495
Pretorius M. L., Knigge C., O'Donoghue D., Henry J. P., Gioia I. M., Mullis C. R., 2007b, MNRAS, 382, 1279
Pretorius M. L., Knigge C., Schwope A. D., 2013, MNRAS, 432, 570
Ramsay G., Schreiber M. R., Gänsicke B. T., Wheatley P. J., 2017, A&A, 604, A107
Ramsay G. et al., 2018, A&A, 620, A141
Rappaport S., Verbunt F., Joss P. C., 1983, ApJ, 275, 713
Richards G. T. et al., 2002, AJ, 123, 2945
Ritter H., Kolb U., 2003, A&A, 404, 301
Rixon G. et al., 2014, Astron. Telegram, 6593, 1
Robinson E. L. et al., 1995, ApJ, 443, 295
Saito R. K., Baptista R., 2006, AJ, 131, 2185
Schenker K., King A. R., Kolb U., Wynn G. A., Zhang Z., 2002, MNRAS, 337, 1105
Schmidt G. D., Stockman H. S., 2001, ApJ, 548, 410
Schmidt G. D., Szkody P., Smith P. S., Silber A., Tovmassian G., Hoard D. W., Gänsicke B. T., de Martino D., 1996, ApJ, 473, 483
Schneider D. P. et al., 2010, AJ, 139, 2360
Schreiber M. R. et al., 2010, A&A, 513, L7
Schreiber M. R., Zorotovic M., Wijnen T. P. G., 2016, MNRAS, 455, L16
Schwope A. D., 2018, A&A, 619, A62
Schwope A. D., Schwarz R., Greiner J., 1999, A&A, 348, 861
Shappee B. J. et al., 2014, ApJ, 788, 48
Sherrington M. R., Jameson R. F., Bailey J., Giles A. B., 1982, MNRAS, 200, 861
Sion E. M., 1995, ApJ, 438, 876
Sion E. M., Cheng F. H., Long K. S., Szkody P., Gilliland R. L., Huang M., Hubeny I., 1995, ApJ, 439, 957
Sion E. M., Szkody P., Cheng F., Gänsicke B. T., Howell S. B., 2003, ApJ, 583, 907
Skrutskie M. F. et al., 2006, AJ, 131, 1163
Smith A. J., Haswell C. A., Hynes R. I., 2006, MNRAS, 369, 1537
Soderblom D. R., Hillenbrand L. A., Jeffries R. D., Mamajek E. E., Naylor T., 2014, in Beuther H., Klessen R. S., Dullemond C. P., Henning T., eds, Protostars and Planets VI. University of Arizona Press, Tucson, AZ, p. 219
Sproats L. N., Howell S. B., Mason K. O., 1996, MNRAS, 282, 1211
Spruit H. C., Ritter H., 1983, A&A, 124, 267
Steeghs D., Howell S. B., Knigge C., Gänsicke B. T., Sion E. M., Welsh W. F., 2007, ApJ, 667, 442
Suleimanov V. F., Doroshenko V., Werner K., 2019, MNRAS, 482, 3622
Sulkanen M. E., Brasure L. W., Patterson J., 1981, ApJ, 244, 579
Szkody P., Silber A., 1996, AJ, 112, 289
Szkody P. et al., 2002, AJ, 123, 430
Szkody P. et al., 2003, AJ, 126, 1499
Szkody P. et al., 2004, AJ, 128, 1882
Szkody P. et al., 2005, AJ, 129, 2386
Szkody P. et al., 2006, AJ, 131, 973
Szkody P. et al., 2007, AJ, 134, 185
Szkody P. et al., 2009, AJ, 137, 4011
Szkody P. et al., 2010, ApJ, 710, 64
Szkody P. et al., 2011, AJ, 142, 181
Szkody P., Mukadam A. S., Sion E. M., Gänsicke B. T., Henden A., Townsley D., 2013, AJ, 145, 121
Taylor M. B., 2005, in Shopbell P., Britton M., Ebert R., eds, ASP Conf. Ser. Vol. 347, Astronomical Data Analysis Software and Systems XIV. Astron. Soc. Pac., San Francisco, p. 29
Thomas H.-C., Beuermann K., 1998, in Breitschwerdt D., Freyberg M. J., Truemper J., eds, Lecture Notes in Physics, Vol. 506, The Local Bubble and Beyond. Springer-Verlag, Berlin, p. 247
Thorstensen J. R., 2003, AJ, 126, 3017
Thorstensen J. R., Lépine S., Shara M., 2008, AJ, 136, 2107
Thorstensen J. R., Schwarz R., Schwope A. D., Staude A., Vogel J., Krumpe M., Kohnert J., Nebot Gómez-Morán A., 2009, PASP, 121, 465
Thorstensen J. R., Alper E. H., Weil K. E., 2016, AJ, 152, 226
Toloza O. et al., 2016, MNRAS, 459, 3929
Tonry J. L. et al., 2018, ApJ, 867, 105
Toonen S., Hamers A., Portegies Zwart S., 2016, Comput. Astrophys. Cosmol., 3, 6
Tout C. A., Wickramasinghe D. T., Liebert J., Ferrario L., Pringle J. E., 2008, MNRAS, 387, 897
Townsley D. M., Bildsten L., 2003, ApJ, 596, L227
Townsley D. M., Bildsten L., 2004, ApJ, 600, 390
Townsley D. M., Gänsicke B. T., 2009, ApJ, 693, 1007
Unda-Sanzana E. et al., 2008, MNRAS, 388, 889
van Spaandonk L., Steeghs D., Marsh T. R., Parsons S. G., 2010, ApJ, 715, L109
Wade R. A., Horne K., 1988, ApJ, 324, 411
Warner B., 1987, MNRAS, 227, 23
Warner B., 1995, Cataclysmic Variable Stars, Cambridge Astrophysics Series No. 28. Cambridge Univ. Press, Cambridge
Watson C. L., Henden A. A., Price A., 2006, Proc. Soc. Astron. Sci. 25th Annu. Symp. Telesc. Sci., Big Bear, CA, p. 47
Wijnen T. P. G., Zorotovic M., Schreiber M. R., 2015, A&A, 577, A143
York D. G. et al., 2000, AJ, 120, 1579
Zharikov S. V. et al., 2008, A&A, 486, 505
Zharikov S. V., Tovmassian G., Aviles A., Michel R., Gonzalez-Buitrago D., García-Díaz M. T., 2013, A&A, 549, A77
Zorotovic M., Schreiber M. R., Gänsicke B. T., 2011, A&A, 536, A42
Zorotovic M. et al., 2016, MNRAS, 457, 3867
Zorotovic M., Schreiber M. R., 2017, MNRAS, 466, L63

APPENDIX A: FLARING RED DWARFS

12 objects in our sample are located on the main sequence or very close it (open and yellow diamonds in Fig. 1). These objects are often classified as CV candidates because they have shown some transient phenomena that have been interpreted as a likely dwarf nova outburst. However, these systems are much redder than the typical CVs and it is therefore more likely that they are actually flaring red dwarfs. This is the case, for example, of MASTER OT J143453.02+023616.1 and MASTER OT J120525.84+621743.3: their SDSS spectra confirm their red dwarf nature (top and middle panels of Fig. A1). The remaining 10 systems have similar colours and we conclude that they are also flaring red dwarfs.

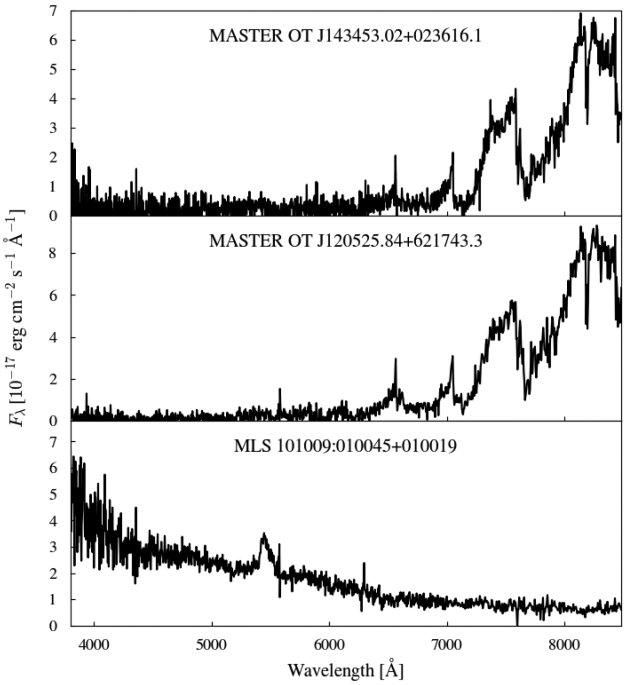

Figure A1. Sample systems reported as CV candidates in the literature. The SDSS spectra reveal that they are actually flaring red dwarfs (top and middle panels) and a quasar (bottom panel).

APPENDIX B: YOUNG STELLAR OBJECTS

Three CV candidates, SSS J155929.1−223618 (Watson et al. 2006), Larin 2 (Denisenko & Larin 2018; Larin et al. 2018), and SSS J035055.8−204817, show particularly red colours but have also a *Galex* detection. Larin et al. (2018) suggested that Larin 2 could be a long-period magnetic CV with a large infrared contribution from the secondary. Later on, Denisenko (2018) argued that wind-driven accretion is going on in this system, where the wind circularization radius is smaller than the Roche lobe radius.

We acquired VLT/X-shooter and William Herschel Telescope/Intermediate-dispersion Spectrograph and Imaging System (WHT/ISIS) spectroscopy for these systems, as well as one SOAR spectrum for SSS J035055.8−204817 (Fig. B1), where we detected the presence of the lithium absorption line at 6707 Å. Lithium is expected to be depleted once the core is hot enough for it to be burnt, and since low-mass stars at this stage are fully convective, its presence in the stellar photosphere suggests youth (Soderblom et al. 2014). Moreover, the forbidden lines of [O I] (5577 and 6300 Å) and [S II] (6730 Å) are commonly observed in young stellar objects (YSOs; Fang et al. 2018) but not in CVs. Finally, the metal emission lines are much narrower than the hydrogen lines and these different line widths suggest that the former arise from a hot corona close to the stellar surface while the latter originate far out in the magnetosphere (Hamann & Persson 1992). We therefore concluded that both systems are likely YSOs (brown diamonds in Fig. 1).

Recently, Denisenko & Larin (2018) identified another CV candidate within 150 pc, DDE 158, owing to its colours and variability properties similar to those of Larin 2. Similarly to

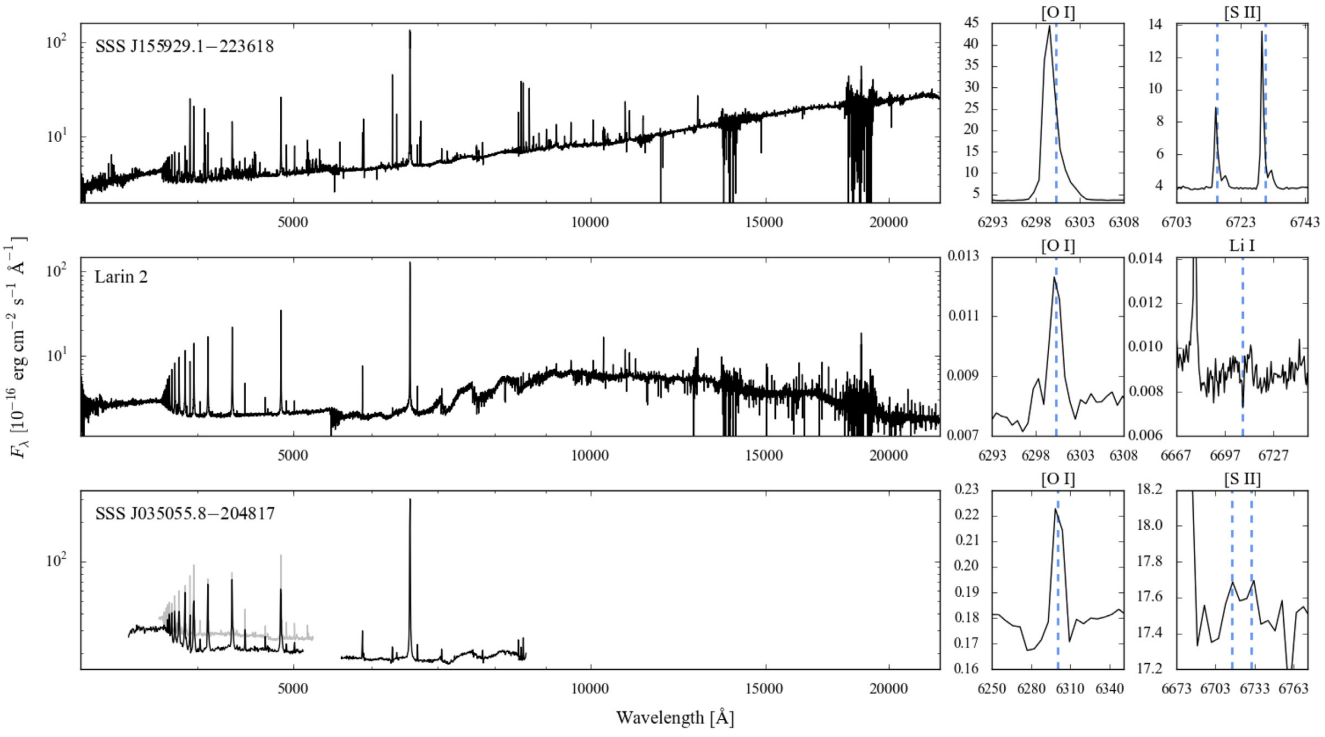

Figure B1. VLT/X-shooter (top and middle panels), SOAR (grey, bottom panel), and WHT/ISIS (black, bottom panel) spectra of three YSOs that have been mistakenly classified as CVs (Watson et al. 2006; Larin, Denisenko & Pogrebisskiy 2018). In all the three systems, the metal emission lines are much narrower than the hydrogen lines, suggesting that the former arise from a hot corona close to the stellar surface while the latter originate far out in the magnetosphere. The panels on the left show a zoom in the regions in which Li I and/or the forbidden lines of [O I] (6300 Å) and [S II] (6730 Å) are detected, which are all characteristic of YSOs.

SSS J155929.1−223618, Larin 2, and SSS J035055.8−204817, the SOAR spectrum of DDE 158 presented in the vsnet-alert #23884 is characterized by metal emission lines narrower than the hydrogen ones, suggesting that they do not originate in a typical CV accretion disc. The non-detection of the forbidden [O I] (5577 Å) line does not allow to rule out a YSO (as suggested in the vsnet-alert #23884) since several YSOs in which this feature has not been detected (even in medium-resolution spectra; see e.g. Natta et al. 2014; Nisini et al. 2018; Banzatti et al. 2019) are known. Finally, the red portion of the spectrum resembles the emission of an M-dwarf star. If DDE 158 was a CV, a secondary star of such spectral type would imply the presence of a white dwarf as hot as $\gtrsim$15 000 K. Given the distance as derived from the *Gaia* parallax ($\simeq$103 pc), such white dwarf would contribute significantly to the overall system emission, causing the spectrum to be much bluer than actually observed. We can thus conclude that also DDE 158 is likely another YSO and therefore we do not include it in our sample.

APPENDIX C: OTHER NON-CV SYSTEMS

Three systems listed in the literature as CVs, SDSS J121929.46+471522.8 (Szkody et al. 2006), NSV 15401 (Downes et al. 2001), and Gaia14abg (Rixon et al. 2014), are actually single white dwarfs.

The SDSS spectrum of SDSS J121929.46+471522.8 shows a blue continuum and a weak emission line at $\lambda = 6539.4$ Å but no absorption and/or emission lines typical of a CV (Fig. C1). This is likely a cold ($T_{\rm eff} \simeq 8000$ K) white dwarf whose atmosphere is dominated by helium, which explains the absence of absorption features. The origin of the emission is, however, unclear. Its wavelength seems to suggest that it arises from an O II transition. However, this is quite unlikely because (i) the formation of O II lines requires much higher temperatures than the one we estimated for SDSS1219 and (ii) many other stronger O II lines should be detected in the spectrum. Contamination from a nearby fibre in the SDSS plate, centred on to a source showing strong emission in this wavelength, is more likely the origin of the observed emission in SDSS1219.

The spectrum of NSV 15401 (also known as Lan 159) presented by Lépine et al. (2011, see their fig. 2) clearly show that this is a single white dwarf, while Gaia14abg was among the first objects identified by the *Gaia* alerts and was affected by a cross-matching problem.

We also discarded five detached binaries (Ret1 REF, BPM 18764 REF), one pre-polar (WX LMi), and MLS 101009:010045+010019, whose SDSS spectrum shows that this system is actually a quasar (bottom panel of Fig. A1).

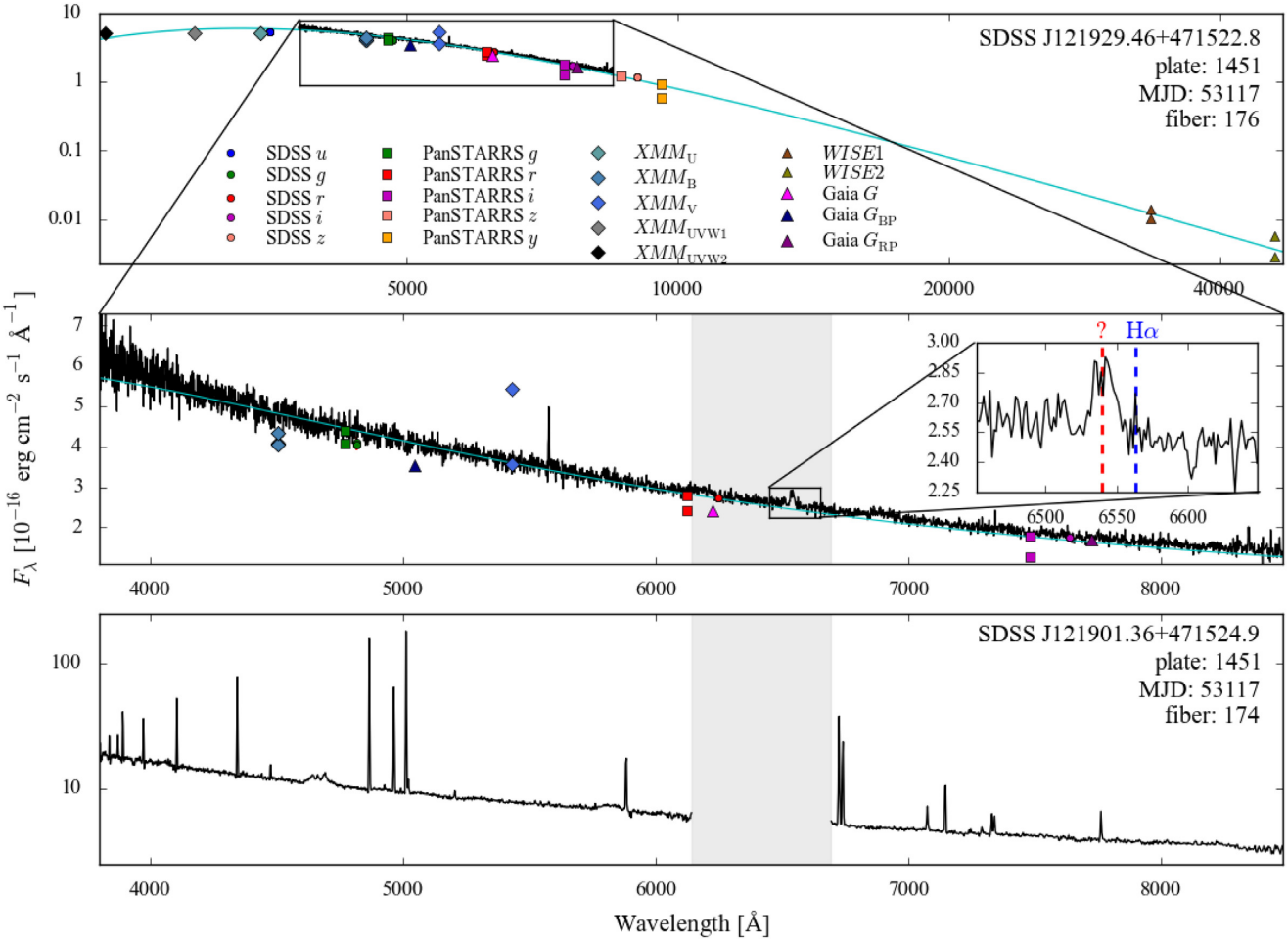

Figure C1. Photometric SED (top) and SDSS spectrum (middle) of SDSS1219 along with a blackbody of $T_{\rm eff} = 8000$ K. In the bottom panel is shown the spectrum of a galaxy observed by a nearby fibre on the same SDSS plate. This galaxy saturated the SDSS detector in the wavelength region (grey band, also highlighted in the middle panel) in which the emission lines are observed in SDSS1219 and it is most likely the origin of this anomalous feature.

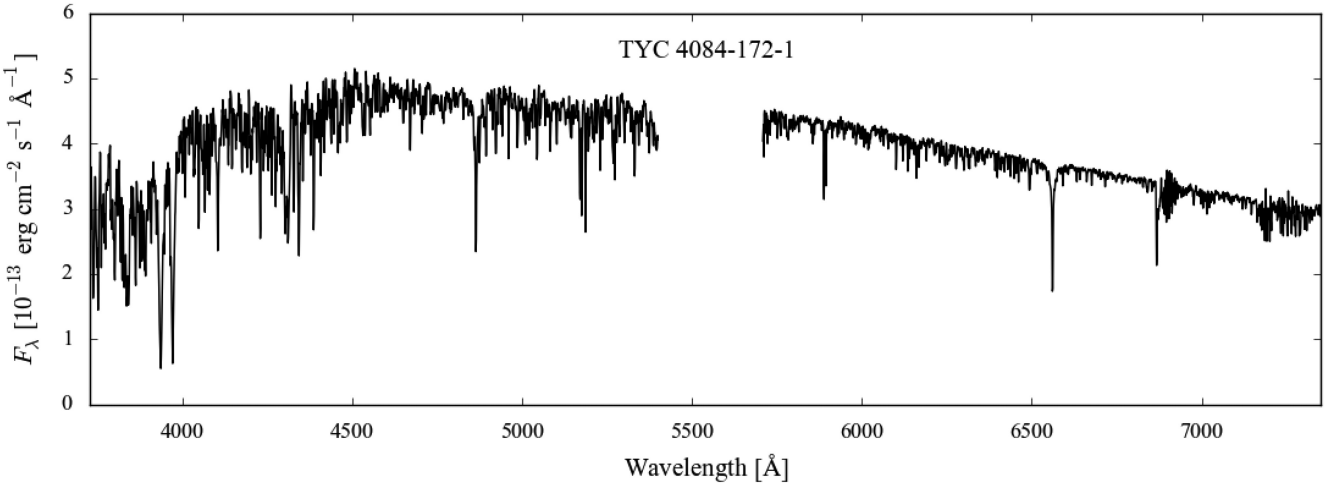

Figure C2. WHT/ISIS spectrum of TYC 4084-172-1, a G3V star (Frasca et al. 2018), located 2.2 pc away from *Gaia* J051903.99+630340.4.

APPENDIX D: NEW CVS FROM GAIA

We observed *Gaia* J051903.99+630340.4 with the ISIS spectrograph mounted on the WHT in La Palma (Spain). We used a 1.2 arcsec slit combined with the R600B and R600R gratings, centred at 4540 Å and 6561 Å and providing a nominal spectral resolution of $R \simeq 2000$ and $R \simeq 4000$, respectively. *Gaia* J051903.99+630340.4 shows a spectrum typical of an SU UMa star, dominated by a blue continuum and strong double-peaked Balmer and He I emission lines (top panel of Fig. 2). Although this class of CVs is characterized by relatively short outburst recurrence times (of the order of months up to 1 yr), it is possible that the dwarf nova outbursts of *Gaia* J051903.99+630340.4 have been missed given the presence of the much brighter nearby companion (TYC 4084-172-1, $G = 9.6$ mag,Fig. C2 and Section 7). With the ISIS spectrograph, we also obtained phase-resolved spectroscopic observations. From a fit to the position of the Hα emission, we estimated a $P_{\rm orb} \simeq 126$ min, consistent with the SU UMa classification.

We performed a spectroscopic follow-up of *Gaia* J154008.28−392917.6 using the Goodman spectrograph (Clemens, Crain & Anderson 2004) mounted on the SOAR telescope in Cerro Pachón (Chile). We used a 1 arcsec slit and the red camera to acquire eight spectra of 300 s exposure each, using a 930 line mm^{-1} grating covering the wavelength range 3650–5200 Å. The average spectrum is shown in the bottom panel of Fig. 2. *Gaia* J154008.28−392917.6 resembles a typical low-accreting system, with the signature of both the white dwarf (pressure-broadened Balmer absorption lines) and the accretion disc (double-peaked Balmer emission lines) clearly detected in its spectrum. Given its spectral similarities with other CVs at the period minimum (see e.g. EZ Lyn in Fig. 8), we classified *Gaia* J154008.28−392917.6 as WZ Sge-type CV likely located close to (or even having already evolved through) the period minimum.

Table D1. CVs with unreliable *Gaia* parallaxes (Sections 2.1 and 2.2) and objects within 150 pc that have been mistakenly identified as CVs in the literature. The flags are as follows: FRD, likely flaring red dwarf; SWD, single white dwarf; DB, detached binary; YSO, young stellar object; Q, quasar; AEN, astrometric excess noise greater than 2; SGD, spurious *Gaia* detection.

System	α	δ	ϖ (mas)	σ_ϖ (mas)	Astrometric excess noise	Flag
MASTER OT J015119.13−643046.6	01:51:19.39	−64:30:45.18	25.1	0.3	1.15	FRD
MASTER OT J031121.54−601851.0	03:11:21.43	−60:18:50.24	19.07	0.13	0.96	AEN
OGLE-BLG-DN-0128	17:47:29.66	−34:42:44.55	18	1	2.12	AEN
N SMC 2012	00:32:55.06	−74:20:19.7	14.60	0.09	0.50	SGD
SDSS J121929.46+471522.8	12:19:29.32	+47:15:22.89	14.3	0.1	0.46	SWD
CSS 131106:032129+180827	03:21:28.62	+18:08:27.05	12.8	0.5	1.64	FRD
MASTER OT J020836.79−104018.8	02:08:36.74	−10:40:18.79	12.2	0.4	1.58	FRD
MASTER OT J194753.58−475722.9	19:47:53.60	−47:57:23.14	12	2	10.18	AEN
MASTER OT J072448.87+533952.1	07:24:48.86	+53:39:51.49	10.6	0.1	0.42	FRD
Gaia16bvf	19:25:17.71	+08:39:20.40	10	2	6.69	AEN
V1454 Cyg	19:53:38.50	+35:21:45.62	10.21	1.79	6.8	AEN
WX LMi	10:26:27.52	+38:45:02.01	10.1	0.1	0.22	DB
Gaia14abg	17:30:47.93	+50:00:16.65	9.5	0.1	0.0	SWD
Ret1	03:34:34.43	−64:00:57.88	9.35	0.02	0.14	DB
BPM 18764	08:02:00.41	−53:27:49.36	9.2	0.1	0.3	DB
OGLE-BLG-DN-0040	17:34:23.99	−23:32:44.43	9	1	2.92	SGD
ASASSN-14ib	04:22:12.22	−03:25:13.47	8.98	3.25	2.89	AEN
MASTER OT J143453.02+023616.1	14:34:53.08	+02:36:16.15	8.4	0.6	0.0	FRD
NSV 15401	01:55:10.12	+69:42:40.14	8.32	0.08	0.13	SWD

Table D1 – *continued*

System	α	δ	ϖ (mas)	σ_ϖ (mas)	Astrometric excess noise	Flag
SBS 1316+577A	13:18:00.68	+57:28:04.00	8.23	0.05	0.36	FRD
SSS J035055.8−204817	03:50:56.02	−20:48:15.95	7.98	0.06	0.0	YSO
Larin 2	12:48:50.77	−41:26:54.65	7.95	0.13	0.32	YSO
Gaia17cuc	10:26:20.55	−44:18:49.68	7.8	0.1	0.39	FRD
ASASSN-17eo	20:02:14.34	+31:36:34.66	8	1	3.17	AEN
SSS J162131.9−230140	16:21:31.92	−23:01:40.73	7.3	0.1	0.59	FRD
SSS J155929.1−223618	15:59:29.20	−22:36:17.82	7.1	0.1	0.34	YSO
MASTER OT J100950.32+471815.8	10:09:50.23	+47:18:16.76	7.0	0.3	0.68	FRD
SSS J155147.2−211323	15:51:47.08	−21:13:23.86	6.89	0.13	0.61	FRD
OGLE-GD-ECL-02234	10:45:49.79	−61:29:57.04	6.79	0.08	0.53	FRD
ASASSN-15ep	08:21:06.24	−72:20:12.09	6.2	0.1	0.71	FRD
OGLE-BLG-DN-0428	18:00:11.42	−29:41:38.40	6	1	2.78	SGD
MASTER OT J012916.47+321859.0	01:29:16.48	+32:18:58.84	6	1	2.46	FRD, AEN
NSV 18024	08:44:35.16	−37:58:02.84	6.1	0.9	7.71	AEN
MACHO 401.48296.2600	17:58:32.38	−27:52:44.12	6	1	2.47	AEN
Gaia17brd	20:15:08.25	+20:40:31.19	6	4	3.4	AEN
MASTER OT J140957.49+290922.7	14:09:57.47	+29:09:22.79	5.8	0.6	0.0	FRD
V1419 Aql	19:13:06.79	+01:34:23.24	6	2	5.41	AEN
MASTER OT J120525.84+621743.3	12:05:25.88	+62:17:43.04	5.7	0.5	2.23	FRD, AEN
MASTER OT J020404.19+741804.6	02:04:03.60	+74:18:02.45	5.6	1.3	4.56	AEN
Gaia17cva	19:45:37.72	+28:05:32.88	6	2	1.46	SGD
OGLE-BLG-DN-0266	17:54:53.98	−21:22:40.19	5	2	3.86	AEN
Gaia17aoi	13:24:44.33	−14:23:35.65	5	1	2.45	AEN
OGLE-BLG-DN-0824	18:10:04.90	−29:05:23.58	5	1	3.61	SGD, AEN
CSS 111021:220328+141059	22:03:28.11	+14:11:00.49	4	1	0.0	SGD
OGLE-BLG-DN-0011	17:17:26.01	−28:33:23.79	4	1	4.47	SGD, AEN
MASTER OT J203824.15+174242.3	20:38:24.10	+17:42:43.15	4	2	2.98	AEN
OGLE-BLG-DN-0087	17:43:07.76	−34:19:28.10	3	1	3.2	SGD, AEN
OGLE-BLG-DN-0156	17:49:49.23	−21:22:13.57	3	2	5.32	SGD, AEN
CSS 150422:172535+231215	17:25:34.90	+23:12:14.33	3	3	5.14	AEN
MASTER OT J051042.59+513540.0	05:10:42.60	+51:35:39.82	3	1	3.14	AEN
CSS 081201:213947+170658	21:39:47.16	+17:06:56.53	3	2	1.65	SGD
Gaia16bfi	16:37:08.62	−67:36:56.46	5.1	1.9	4.70	AEN
ASASSN-13cv	22:10:25.35	+30:46:10.06	4.5	0.8	1.19	FRD
OGLE-BLG-DN-0584	18:03:46.14	−27:15:33.70	4.2	0.8	1.74	FRD
ASASSN-17gc	19:51:36.94	−00:59:04.05	4	2	0.71	SGD
ASASSN-16cd	19:06:38.16	+33:09:03.17	3.4	1.5	5.5	SGD, AEN
ASASSN-17nm	09:46:09.11	−57:14:20.41	3.1	1.2	0.0	SGD
Gaia17aok	21:52:55.72	59:18:18.71	3.1	1.2	0.0	SGD
CSS 120313:131043−042600	13:10:42.68	−04:26:00.73	3	2	2.2	AEN
OGLE-BLG-DN-0216	17:52:24.02	−32:16:51.54	2.2	1.5	2.7	SGD, AEN
EL Aql	18:56:01.87	−03:19:18.80	2	3	2.68	AEN
MASTER OT J182201.93+324906.7	18:22:01.80	+32:49:00.57	2.0	2.0	4.85	SGD, AEN
MLS 101009:010045+010019	01:00:44.71	+01:00:18.48	2	2	1.53	Q
EU Cnc	08:51:27.17	+11:46:56.94	2	2	0.0	SGD
OGLE-BLG-DN-0181	17:51:01.18	−29:14:38.30	2	2	2.82	AEN
Gaia17afs	17:35:17.86	+01:32:48.79	1.1	1.9	3.0	SGD, AEN
OGLE-BLG-DN-0054	17:38:24.00	−21:54:26.87	2	2	2.13	AEN
DO Vul	19:52:10.72	+19:34:42.14	0.8	2	4.78	AEN
Gaia17bqf	19:59:19.93	+16:24:40.31	−0.2	2	3.07	AEN
V1722 Aql	19:14:09.74	+15:16:38.25	−1	3	3.07	SGD, AEN

Table D2. CV and CV candidates with parallaxes $\varpi + 3\sigma_\varpi \geq 6.66$ mas that are located further than 150 pc.

System	α	δ	ϖ (mas)	σ_ϖ (mas)	Distance (pc)	$P(d <$ 150 pc) (per cent)
V1108 Her	18:39:26.14	+26:04:09.96	6.6	0.1	152 ± 3	0.24
EK TrA	15:14:00.10	−65:05:36.65	6.58	0.04	152 ± 1	0.02
BZ UMa	08:53:44.22	+57:48:40.35	6.56	0.06	153 ± 1	0.04
EI Psc	23:29:54.17	+06:28:12.11	6.55	0.07	153 ± 2	0.04

Table D2 *– continued*

System	α	δ	ϖ (mas)	σ_{ϖ} (mas)	Distance (pc)	$P(d <$ 150 pc) (per cent)
MASTER OT J050806.84+712352.0	05:08:06.78	+71:23:51.69	6.5	2.8	487^{+489}_{-255}	0.04
FL Psc	00:25:11.04	+12:17:11.81	6.5	0.1	154 ± 3	0.11
V348 Pav	19:56:48.05	−60:34:30.00	6.48	0.08	154 ± 2	0.006
ASASSN-16jg	14:45:35.72	−39:20:26.73	6.4	0.3	158^{+9}_{-8}	0.17
1RXS J083842.1−282723	08:38:43.33	−28:27:00.95	6.4	0.1	157 ± 3	0.004
SDSS J150551.58+065948.7	15:05:51.61	+06:59:48.49	6.3	0.4	162^{+13}_{-11}	0.14
EF Eri	03:14:13.41	−22:35:43.77	6.3	0.3	161 ± 7	0.05
MASTER OT J220559.40−341434.9	22:05:59.47	−34:14:34.15	6.2	0.3	161 ± 7	0.04
CSS 081221:050716+125314	05:07:16.24	+12:53:14.16	5.4	2.3	485^{+467}_{-237}	0.02
ASASSN-18bh	01:09:52.87	+47:57:11.11	5.2	1.7	361^{+354}_{-146}	0.02
ASASSN-14ip	20:50:23.43	−48:37:13.71	5.0	1.1	253^{+115}_{-60}	0.01
V498 Hya	08:45:55.06	+03:39:29.28	4.9	2.0	469^{+446}_{-217}	0.01
ASASSN-15td	12:15:13.70	−01:46:41.56	4.9	2.3	527^{+478}_{-255}	0.01
OGLE-BLG-DN-0183	17:51:05.70	−28:03:37.84	4.8	1.8	440^{+416}_{-193}	0.01
ASASSN-16ee	08:35:42.43	−31:21:47.92	4.5	1.3	335^{+254}_{-110}	0.006
CSS 170417:080539+354055	08:05:38.98	+35:40:54.94	4.3	1.7	461^{+413}_{-196}	0.006
ASASSN-13bd	23:59:58.00	−12:54:32.68	4.3	2.2	575^{+485}_{-271}	0.007
SDSS J125641.29−015852.0	12:56:41.29	−01:58:51.74	4.0	1.1	350^{+202}_{-96}	0.0007
CSS 080927:212522−102627	21:25:21.76	−10:26:28.18	4.0	1.6	471^{+404}_{-194}	0.003
MASTER OT J122126.39−311248.3	12:21:26.40	−31:12:48.49	3.8	1.0	363^{+217}_{-104}	0.0002
CSS 111103:074400+415504	07:44:00.47	+41:55:03.56	3.7	2.4	636^{+499}_{-295}	0.004
IK Leo	10:21:46.45	+23:49:25.91	3.6	1.4	499^{+402}_{-198}	0.0008
ASASSN-15rj	02:59:38.35	+44:57:04.77	3.6	1.6	529^{+429}_{-220}	0.001
MASTER OT J070740.72+702630.0	07:07:40.55	+70:26:30.30	3.5	1.1	416^{+287}_{-135}	0.0002
ASASSN-15ef	16:49:40.59	−17:50:09.72	3.5	1.6	549^{+444}_{-234}	0.001
CSS 110124:032934+182530	03:29:33.92	+18:25:29.57	3.5	1.1	406^{+265}_{-126}	0.0001
ASASSN-17jf	20:29:17.10	−43:40:19.18	3.5	1.1	426^{+297}_{-140}	0.0001
ASASSN-17mw	02:49:07.33	+48:51:01.16	3.5	1.1	408^{+265}_{-127}	0.00009
Gaia16apf	00:34:33.39	+54:28:42.04	3.5	1.3	488^{+381}_{-186}	0.0004
ASASSN-15gm	19:37:13.59	−22:57:06.31	3.5	1.6	544^{+435}_{-226}	0.0009
ASASSN-16jb	17:50:44.96	−25:58:37.45	3.42	1.2	456^{+334}_{-160}	0.0002
ASASSN-16do	06:34:12.71	−32:59:49.49	3.1	1.3	525^{+392}_{-198}	0.0001
ASASSN-13ck	00:11:33.73	+04:51:22.43	3.1	1.6	590^{+452}_{-247}	0.0005
ASASSN-15px	23:08:57.87	−65:59:32.49	3.1	1.3	547^{+413}_{-214}	0.0002
CSS 110406:152159+261223	15:21:58.84	+26:12:23.30	2.7	2.1	689^{+499}_{-303}	0.001
CSS 101108:022436+372021	02:24:36.44	+37:20:21.40	2.7	1.8	671^{+485}_{-287}	0.0005
KK Cnc	08:07:14.25	+11:38:12.32	2.5	1.6	670^{+476}_{-278}	0.0002
ASASSN-16jk	15:40:24.84	+23:07:50.86	2.5	1.4	655^{+457}_{-260}	0.00004
MASTER OT J152701.21−314433.6	15:27:01.25	−31:44:35.30	2.5	1.5	667^{+468}_{-270}	0.00008
ASASSN-15aw	01:57:46.15	+51:10:23.88	2.4	1.7	695^{+487}_{-292}	0.0002
CSS 100108:081031+002429	08:10:30.61	+00:24:28.32	2.4	2.2	716^{+504}_{-312}	0.0008
ASASSN-15nf	20:12:42.71	+15:44:44.92	2.4	2.4	724^{+509}_{-319}	0.001
CSS 110430:091710+314309	09:17:09.87	+31:43:07.59	2.3	1.5	686^{+472}_{-376}	0.00005
ASASSN-17bi	02:16:05.42	+68:39:03.61	2.3	1.5	694^{+477}_{-282}	0.00007
CSS 090928:030141+241541	03:01:40.52	+24:15:41.35	2.3	2.5	732^{+511}_{-323}	0.002
ASASSN-14kk	01:32:02.78	−10:43:57.72	2.3	1.5	689^{+471}_{-276}	0.00004
MASTER OT J211855.08+280314.9	21:18:55.10	+28:03:15.39	2.2	3.1	744^{+520}_{-335}	0.002
SSS 110125:103550−424610	10:35:49.64	−42:46:10.14	2.1	2.2	741^{+508}_{-320}	0.0006
CSS 150822:232026+221833	23:20:26.23	+22:18:34.05	0.3	3.0	814^{+523}_{-346}	0.0007
CSS 090926:230711+294010	23:07:11.34	+29:40:11.33	0.2	2.2	857^{+519}_{-344}	0.00007

Table D3. CVs with pre-*Gaia* distance estimates $d \leq 150$ pc.

System	*Gaia* DR2 ID	$P_{\rm orb}$ (min)	Distance (pc)	Method	Reference	*Gaia* G (mag)	$G_{\rm BP}$ (mag)	$G_{\rm RP}$ (mag)	ϖ (mas)	σ_{ϖ} (mas)	Distance (pc)
WZ Sge	1809844934461976832	81.63	$43.30^{+1.60}_{-1.50}$	a	1	15.21	15.21	15.06	22.16	0.04	45.13 ± 0.08
AY Lyr	2096934223687181696	105.55	52	c	2	17.93	17.96	17.50	2.22	0.13	452^{+32}_{-22}
XZ Eri	5097770801875122432	88.7	66	c	2	19.25	19.28	19.00	3.0	0.3	331^{+44}_{-24}
VW Hyi	4653893040002306432	106.95	64^{+20}_{-17}	e	3	13.84	13.94	14.45	18.53	0.02	53.96 ± 0.06
EX Hya	6185040879503491584	98.26	64.5 ± 1.2	a	4	13.21	13.23	12.88	17.56	0.04	56.95 ± 0.13
GD 552	2208124536065383424	102.73	74 ± 4	e	5	16.46	16.46	16.18	12.35	0.05	81.0 ± 0.3
QZ Vir	3800596876396315648	84.70	76	c	2	16.06	16.12	15.76	7.81	0.07	128 ± 1
AM Her	2123837555230207744	185.65	79^{+8}_{-6}	a	1	13.58	13.86	12.85	11.40	0.02	87.76 ± 0.14
1RXS J105010.3−140431	3750072904055666176	88.56	80 ± 20	e	5	17.17	17.21	17.08	9.14	0.11	109 ± 1
AR UMa	783921244796958208	115.92	86^{+10}_{-8}	a	6	16.26	16.35	15.78	9.87	0.12	101 ± 1
V455 And	1920126431748251776	81.08	90 ± 15	b	7	16.06	16.13	15.71	13.24	0.06	75.5 ± 0.3
ASASSN-14ag	3071240270519385856	86.85	90	e	8	16.18	16.17	15.70	5.63	0.09	178 ± 3
IX Vel*	5515820034889610112	279.25	96 ± 1	a	9	9.32	9.34	9.27	11.04	0.03	90.6 ± 0.2
VY Aqr	6896767366186700416	90.85	97^{+15}_{-12}	a	1	16.86	16.96	16.44	7.24	0.14	138 ± 3
U Gem	674214551557961984	254.74	97 ± 7	c	10	13.91	14.38	13.11	10.71	0.03	93.3 ± 0.3
IGR J18308−1232	4153024090088033280	–	100	c	11	17.65	18.07	16.89	0.49	0.15	1595^{+514}_{-193}
V426 Oph	4471872295941149056	410.83	100	e	12	12.37	12.65	11.77	5.20	0.04	192.5 ± 1.5
WW Cet	2427474150870397056	253.15	100	c	2	13.55	13.65	12.96	4.59	0.05	218 ± 2
OY Car	5242787486412627072	90.89	100	c	13	15.62	15.64	15.21	11.01	0.03	90.8 ± 0.2
V2051 Oph	4111991385628196224	89.90	102 ± 16	e	5	15.37	15.46	14.87	8.90	0.07	112.4 ± 0.9
AE Aqr*	4226332451596335616	592.78	102^{+42}_{-23}	a	1	10.95	11.47	10.26	10.97	0.06	91.2 ± 0.5
GW Lib	6226943645600487552	76.78	104^{+30}_{-20}	a	1	16.49	16.49	16.32	8.87	0.08	113 ± 1
DI UMa	1013298268207936128	78.59	107	c	2	17.75	16.86	16.82	1.46	0.08	685^{+43}_{-31}
V3885 Sgr*	6688624794231054976	298.31	110 ± 30	a	14	10.25	10.28	10.16	7.54	0.08	133 ± 1
HU Aqr	6911950900211768704	125.02	111	c	2	16.47	16.66	15.88	5.20	0.06	192 ± 2
Z Cha	5210507882302442368	107.28	112 ± 8	c	10	15.85	15.94	15.19	8.66	0.12	115 ± 1
AH Eri	3176908972944418816	344.30	113	c	2	17.46	17.85	16.75	0.82	0.09	1129^{+134}_{-80}
EF Eri	5099482805904892288	81.02	113^{+19}_{-16}	a	1	18.21	18.17	18.11	6.3	0.3	161 ± 7
BK Lyn	702296666944246784	107.97	114	c	2	14.52	14.48	14.45	1.98	0.07	505^{+20}_{-16}
SS Cyg*	1972957892448494592	396.19	114 ± 2	a	15	11.69	12.11	10.95	8.72	0.05	114.6 ± 0.6
ST LMi	3996419759863758592	113.89	115^{+21}_{-22}	b	16	16.13	–	–	8.83	0.08	113 ± 1
DH Aql	4200218019655998720	–	116	c	2	17.97	18.28	17.43	3.6	0.2	282^{+18}_{-13}
IQ Eri	5078976609103251456	–	116^{+116}_{-58}	e	3	17.18	17.11	16.85	5.19	0.17	193^{+7}_{-6}
IP Peg	2824150286583562496	227.82	124	e	12	14.71	15.27	13.88	7.08	0.05	141 ± 1
VV Pup	5719598950133755392	100.44	124^{+17}_{-14}	a	6	15.93	16.04	15.48	7.30	0.05	137 ± 0.9
MR Ser	1203639265875666304	113.47	126^{+14}_{-12}	a	6	16.23	16.47	15.64	7.59	0.05	131.8 ± 0.9
TV Col	2901783160488793728	329.18	128 ± 1	a	17	13.93	14.03	13.61	1.95	0.02	512 ± 4
IGR J17195−4100	5959894875620104064	240.34	130	c	11	15.33	15.55	14.75	1.53	0.04	653^{+30}_{-27}
EQ Cet	5041907811522399488	92.82	130	c	18	17.34	17.41	16.78	3.51	0.11	285^{+10}_{-8}
BL Hyi	4697621824327141248	113.64	130	c	19	17.25	17.45	16.70	7.65	0.07	131 ± 1
BW Scl	2307289214897332480	78.23	131 ± 18	b	20	16.26	16.26	16.10	10.60	0.10	94.4 ± 0.9
HT Cas	426306363477869696	106.05	131^{+22}_{-17}	a	8	16.35	16.48	15.80	7.07	0.06	141 ± 1
RX And	3745102948302449 92	302.24	135	e	12	13.17	13.38	12.50	5.03	0.05	199 ± 2
V406 Vir	3681313024562519552	80.52	140 ± 35	e	5	17.72	17.71	17.55	5.91	0.16	169 ± 5
V834 Cen	6096905573613586944	101.52	144^{+18}_{-23}	b	16	16.66	16.82	16.07	8.9	0.2	113 ± 3
V405 Peg	2838503311371673472	255.81	149	a	21	15.28	16.05	14.29	5.78	0.06	173 ± 2
V2301 Oph	4476137370261520000	112.97	150	b	22	16.75	16.94	15.86	8.24	0.08	121 ± 1
SX LMi	733329416268149376	96.72	150	c	2	16.69	16.77	16.30	3.08	0.12	325^{+14}_{-11}
CU Vel	5524430207364715520	113.04	150 ± 50	b	23	16.71	16.93	16.15	6.29	0.06	159 ± 2

Notes. Systems highlighted with an asterisk have a parallax measurement from *Gaia* DR1 (Ramsay et al. 2017), but we do not report them in this table since they do not represent a pre-*Gaia* distance determination. The method abbreviations recall the list in Section 4. The distances reported in the last column have been determined from the *Gaia* parallaxes as described in Section 3.

References: (1) Thorstensen (2003), (2) Sproats, Howell & Mason (1996), (3) Pretorius & Knigge (2012), (4) Beuermann et al. (2003), (5) Patterson (2011), (6) Thorstensen et al. (2008), (7) Araujo-Betancor et al. (2005a), (8) Thorstensen et al. (2016), (9) Linnell et al. (2007), (10) Beuermann (2006), (11) Bernardini et al. (2012), (12) Warner (1987), (13) Sherrington et al. (1982), (14) Linnell et al. (2009), (15) Miller-Jones et al. (2013), (16) Araujo-Betancor et al. (2005b), (17) McArthur et al. (2001), (18) Schwope, Schwarz & Greiner (1999), (19) Beuermann et al. (1985), (20) Gänsicke et al. (2005), (21) Thorstensen et al. (2009), (22) Szkody & Silber (1996), and (23) Gänsicke & Koester (1999).

This paper has been typeset from a TEX/LATEX file prepared by the author.